Dear Editors and Reviewers,

Thank you for your detailed comments and suggestions about our manuscript entitled "Dense point cloud acquisition with a low-cost Velodyne VLP-16". The paper has been thoroughly revised according to your recommendations. In particular, we followed the guidelines below:

- The introduction and literature review were refined in relation to studies focusing on scanner calibration and error modeling as well as similar studies.

- Comparison of the scanner with a higher precision scanner has been added and allowed for a more complex analysis than that of a reference design.

- Repeatability tests were carried out 8 times to assess the temporal stability of the developed device in order to clear the raised doubts by reviewer #1 regarding the validity of the calibration values and therefore the suitability of the device for actual applications.

- The figures have been improved in line with the reviewers' remarks.

- The configuration and design of our system as well as a complete definition of the terminologies used have been added.

In the following point-by-point replies, black text denotes a reviewer comment, blue text denotes our response to the comment and red text our corrections.

Hoping that these responses will fulfill your expectations, Best regards,

Jason Bula, Gregoire Mariethoz and Marc-Henri Derron.

Responses to the comments of Reviewer #1:

I like the idea to create a 3D terrestrial laser scanner from low-cost components. The combination of a profile scanner (e.g. Velodyne) with a rotation drive on a tripod is reasonable but not novel in principle. The authors demonstrate that the concept works in general and they describe the system and the processing scheme adequately. However, I have some critical points to address. Here are the main points which argue for "major revision", other and more detailed comments and suggestions can be found in the attached document.

> We thank the reviewer for the positive feedback on our ideas. All comments are addressed below.

There are other projects where 2D profile scanner used to form a low-cost 3D scanner and this is not mentioned at all. Some examples are given as comments in the attached commented document.

> A complete review of the different projects developing low-cost lidar scanner of similar as the one developed in this study has been added in the revised version.

There are several publications on geometric modeling and calibration of terrestrial 3D laser scanners. The authors give no credit on that and does ignore these approaches completely. They develop there own geometric model and calibration instead, which is at least questionable (as they conclude by themselves)

> Our research focuses on the use of a low-cost lidar scanner (Velodyne VLP-16) to create a terrestrial laser scanner (TLS). Our goal was to recreate a dense scan by positioning the lidar on a rotating motor. The continuous recording of the points coupled with the rotation of the motor allowed us to recreate a dense 360-degree image.

> The term calibration may be inappropriate; we changed with the term adjustment. We assumed that the lidar system sold by Velodyne was calibrated (will be clearer in the revised version). We have chosen to use our own geometric model based mainly on the assembly of the motor and lidar, as the system components (lidar, motor, ball head) are disassembled after each use. Our research has shown that when the system is reassembled or moved, the parameters governing the reconstruction of a dense scan vary, which implies the need to perform an adjustment (automatic in post-processing) after each new measurement.

> This is why the use of an on-site method of calibration/adjustment (use of target, planar feature, or a direct georeferencing with GNSS) is in our opinion not optimal for such a system because it would imply to renew the approach after each measurement. Additionally, it would make our device more expensive.

> Adjustment could be avoided after each measurement if the system components were welded together. However, we wanted to keep the possibility to separate these elements in order to use the lidar for other projects for example. This will be discussed in the revised manuscript.

The above mentioned geometric models as well mostly base on the know error sources of geodetic instruments (theodolite, total station) which have the same structure as terrestrial 3D laser scanners and also the presented device. The parameters are different axis and eccentricity errors, where equations are presented in geodetic standard literature. Why is that not considered? There are no equations given at all.

The evaluation part is not very scientific to assess the performance of the system. It seems the system works, and the authors claim it works well for their applications. However, the readers might like to wish a better proof in terms of a thorough scientific analysis in order to be able to assess the suitability of the instrument for other applications as well. To mention some examples: the analysis bases only on a fitted plane to the point cloud of the floor and does not cover the whole field of view. There are only 4 scans which produced completely different calibration values and there is no hint on the parameter's significance. The reproducibility test compares only 2 scans for different scanning speeds, which does not really allow for conclusions. Why the data are not compared to a reference model or reference scan with a superior precision? Some illustrating figures (color-coded point cloud comparison) would be more than desirable (even though only with the fitted plane and the floor points). The most often used approach would be the use of 3D check points and a thorough comparison of the coordinates (RMSE). There are some more comments within the attached document.

Our study was carried out to determine if it is possible to get a TLS for a lower price while still being able to disassemble the system but we agree that the system evaluation tests are indeed incomplete. Concerning the reproducibility test; We carried out 8 of them to evaluate the temporal stability of the developed device
The few tests carried out allowed us to see that the system is unstable (adjustment necessary after each measurement), which we address with a post-processing adjustment procedure. A comparison with a high accuracy scanner and 3d check points has been added in the revised version.
However, tests in known environments will be an indication of the quality of the fit because the nature of the scanned scene influences the quality of the adjustment (the algorithm used to find the alpha1 and alpha2 parameters is less powerful when it is about environments with complex characteristics).

I can not really understand why the presented system is always compared to IMU- or SLAM-based mobile scanners. From my point of view this is not reasonable, as MLS and TLS have different advantages and subsequently different applications scenarios. It is obvious that the point cloud of a tripod-based device is more precise as the whole point cloud from one position is within the same coordinate system per definition than a handheld mobile device where each single point has to be tracked. Therefore I would absolutely prefer a comparison with other (maybe "low-cost" 3D scanners), such as Leica BLK 360 oder FARO FocusM 70 (ca. 20.000 $ second

hand below 10.000 $ or for rent 100-200$ per day), this would be more fair in terms of an adequate assessment of the device at hand.

The use of a SLAM system in our study is for the unique purpose of validating the quality of the data. The Geoslam (GeoSLAM ZEB-Revo) allows data acquisition to an accuracy of 1-3 cm according to the manufacturers (3 cm for the VLP-16).

New measurements with Geoslam and a high-precision lidar (Optec IIris 3D) have been carried out in the revised version.

Responses to the comments of Reviewer #2:

This paper shows how a lidar hardware, mass-produced for the autonomous car industry, hence cheap, but not designed for topographic measurements, can be assembled with common equipment to build a tool for dense point clouds generation. This subject is really appealing for many geoscience researchers. You make a point at staying as pratical and low-tech, as well as low-cost, as possible. The core of your contribution resides in determining two unknown values which bias the data: the angle between the local vertical and the scanner's scanning angle origin (alpha-1) and the scanning plane angle (alpha-2) with respect to the supporting platform rotation axis. In essence, the exercise solved expresses a scanner's rotating (time variant) XYZ coordinates into a static (time invariant) cartesian reference frame.

We thank the reviewer for the encouraging comments.

This goal is very valuable. It would further benefit the geoscience community to a higher degree if the resolution code was provided as supplementary material.

The link does not seem to be active on the paper but is available at this GitHub repository : https://github.com/jason-bula/velodyne_tls

The paper is concise. It is appreciable in many respects. This conciseness is however detrimental at times. In particular, the presentation of the equipment and its specific setup is too elusive, and the wording not sufficiently defined. The reader needs to grasp what output data is provided by the Velodyne scanner and by the rotary motor. In what form ? XYZ, time, intensity, polar coordinates? How the synchronization between the platform and the scanner perfomed? These are the prior information for solving the unkonwn variables, but they are not explicit in the text.

More information on the setting and on the data produced by the lidar (coordinate system, signal strength, number of returns, etc.) have been added in the revised version.

A second point is the need to specify the domain of application targetted by this equipment. What would be the required point density and precision to deem the equipment fit for its intended purpose?

Areas of application particularly in geoscience have been added in the revised version. We particularly target applications in rough field conditions, such as for example caves that are difficult to access. In such places there is a likelihood of damage to the equipment due to shocks, water, or dirt, which prevents the use of high-cost equipment.

This being said, I would really like to start testing this Equipment for my own applications and see plenty of usage for underground permanent scanning in

Dangerous areas. This is good job to have tested and published the results.

Specific comments: On the paper structure: The abstract should absolutely state the term Terrestrial Laser Scanner (TLS) so as to understand what range of problems are addressed with this hardware solution. It should also state the point precision and the range within which is achieved (line 6: "good result" must be qualified). And also qualify explictly what you mean by expensive and cheap device. Price is set forward as the core issue? But then there is no extension of what low cost would mean in terms of applications. It opens the door to measuring risky sectors where instrument loss is high but information valuable. It also enables using multiple scanning devices. This is what your contribution opens.

We included details on the applications to risky areas in the revised version.

The introduction does not do justice to your work. The introduction contents does not frame your work properly. An introduction should specify the scientific and technical landscape in which your study is set, establish gaps in previous works, sketch the question that you will solve and evoke the technicalities to solve them. In essence your introductory section contains 3 paragraphs: what is a laser? what properties does a Terrestrial Laser Scanner have? And then, what you have done. The reader does not have a good overview of laser scanning applied to geosciences nor of pending issues that you set out to solve. You evoke issues linked to hardware cost, 3D point cloud density, scanning duration and point cloud accuracy. The logic articulating these 4 ideas however remains elusive.

Here is an attempt at repackaging this introduction. My understanding of your paper is that you try to create an accurate depiction of your 3D environment with a lidar profiler designed for the autonomous car industry. The chosen model is mass-manufactured, hence cheap, but designed to address obstacle avoidance issues, not 3D environment reconstruction. The Velodyne VLP-16 scans 16 parallel profiles in a field of view of +/- 15° above and below the scanning plane, 360° around the scanner's axis. Each lidar profiler is set 2° apart in a plane normal to the profile rotation axis. Your aim is to densify points in the 2° interval using an external rotating plate.

We beefed up the abstract and introduction according to the reviewer's comments. Background material are given, although we want to keep the paper short.

Note that rotating the scanning plane of a profiler is the solution adopted by all TLS manufacturers since the early 2000. The mathematical solution therefore exists somewhere, refering to it may be useful if explicit documentation exists on the matter. But since it may not be clearly exposed by manufacturers, or you may have an original approach, there is value in (re-)exposing the methodology in a free and open access article. To prove your point, you show an implementation with much cheaper hardware than that currently for sale. This option goes with its own issues which you then discuss.

Your list of applications papers is rather short and perhaps not exhaustive enough for pioneering works with laser scanning (references in the end of this review). For TLS applications on landslides and rockfalls, perhaps add citations for Lim et al.

(2005), Dewez et al (2007), Abellan et al. (2009). For permanent laser scanning applications, you cannot miss Williams et al (2018). It is another application where the use your low- cost solution has a future. For mobile laser scanning, there are the studies using boatborne systems e.g. Michoud et al (2015), Feldmann et al (2018). Mobile handheld devices such as Geoslam's Zebedee in different versions was discussed among others by James & Quinton (2014), Chang et al (2016), Dewez et al (2017).

We thank the reviewer for these bibliographical references and other elements, which we added in our revisions.

When it comes to the essence of the paper, the reader is left in the dark on many issues.

A figure decomposing the different reference systems and key variables of the lidar and assemblage would be extremely useful. This will help the reader grasp the essence of the problem. Figure 4 is not sufficient to understand the geometry of the acquisition system. Make it in relation with the terms given in table 1 and 2.

Figure 4 has been merged with Figure 2 to show the details and the geometry of the entire system.

In table 1, What does the vertical angle increment and horizontal angle increment mean? Can you sketch these on a figure ? The issue tackled is that of a moving reference frame. The rotation motion is eccentric and in some non-vertical plane. A clear description of the different reference systems and how they relate to one another would clarify the problem. Please also state what the digital output of the lidar is. Does it output a series of XYZ point coordinates associated with a time stamp for each? Does one have access to the lidar beam index number? Does one have access to the "horizontal" angle? Is there an index point value to know which one of the 1810 angular increment a reflector is related to? In Riegl's vocabulary, the different reference frames are called SOCS (Scanner's Own coordinate system) and PRCS (Project's Reference Coordinate System). Using a similar terminology will perhaps help to clarify the concepts. And even within the SOCS reference frame, there is one associated with the scanner and one relative to the rotary motor rotation. Inside the VLP16 each of the 16 beams scan a circle around a rotation axis clockwise. The direction of each beam diverges by 2 degrees. This divergence make that the lidar traces 16 cones of revolution about a centre. The origin of the circle of revolution (Y axis on figure 4) may be offset. It would be usefull to spell all this out both in text and drawing.

All these points have been clarified in the revised manuscript. Specifically, Table 1 have been amended with details and a new figure combining current figures 2 and 4 better describes the geometry of the system.

I also feel uneasy with undefined terminology which confuse me alot. What is the meaning of "10 frames per second" (line 28)? What is a "frame" in this context?

Does it have a raster meaning ? If it is a 2D grid in some reference frame, which one? Could it be a grid in polar coordinates? In this time-variant system, should I understand a frame as something acquired during a short duration like a photograph? Defining this term will reduce speculations. Line 59: "Each frame is rotated by an angle" How so? Isn't it a continuous rotation? What is a "frame" in this context? What is an image (line 39)? Does it mean a "representation" ? Is it a 2D raster grid with values? Can it just be a vector of polar distance with time? Again, not defining this term leaves the reader speculating

> The reviewer is correct in pointing out that our terminology was confusing. There are indeed no frames as the data are acquired continuously. The lasers rotate at a frequency of 10 Hz, and not at 10 frames per second. What we called a frame is the set of point measured each 1/10 of a second. The terminology has been corrected in the revised manuscript.

Why talk about time lapse (line 58)? Isn't it a continuous acquisition? I understand "lapse" as a series of static snapshots. Do you mean the Syrp Genie motor is stepping by increments? Or is it continuously rotating? Please mention this is in Section 2.3

> This is the time between starting the motor and starting the lidar acquisition. This has been clarified in the revised manuscript.

Calibration (line 88): what do you mean? You are certainly trying to resolve (i) the eccentricity, (ii) the angle between the scanner's origin Y axis and the plumbline vertical, and (iii) the inclination of the scanning plane with respect to the plate rotation axis. Here by vertical I refer to the direction of a plumbline under the scanner, not the abusive "vertical" term used in table 1, which only marks the direction of the rotation axis. The plumbline direction may not coincide with the motor's rotation axis orientation if the tripod head is not level (not discussed but worth mentioning). Please make an explicit note about the abusive use of "vertical" and "horizontal" in table 1. You may very well keep on using vertical and horizontal abusively in the text, but warn the reader you do so.

> The term calibration may be inappropriate. It should be referred to as adjustment of the motor relative to the lidar. This has been clarified in the revised manuscript.

Section 3.3 (line 115) You write that a plane is fitted in the distance range 3-7 m from the lidar. It is probably for this reason that the alpha-1 and alpha-2 determination yield the residual error pattern seen on figure 6b. The two-tailed error pattern gives the impression that the inversion solution was not trying to optimize the appropriate mathematical function. Dropping the negative error branch unilaterally seem not properly justified. You are hiding errors arbitrarily. With this double branching function, computing a moving average would cancel the error

rather than bias things further by using just one branch.

> The moving average is a solution we have considered for this problem, and tests have been carried out but with unsatisfactory results in complex environments. However, it has been chosen to remove the negative error branch in order to preserve details, which a moving average would smooth out. The alpha 1 and alpha 2 parameters are very sensitive and the error intensifies with the scan distance, which makes the interplay of the two patterns complicated.

For a different approach, you may want to look at Chang et al (2016). They based their tests on reconstructing geometrical shapes. In the corridor where the scan is tested, you could have used the planar walls and rectangular section properties to assess lidar "refocussing".

Section 4 Result line 150: Figure 5 is absolutely not visually explicit on a printed version. You try to exhibit cloud roughness in Figure 5a, and how your post-processing (rather than the word "post-treatment") improves results in figure 5b and 5c. Why did you not use Cloud Compare's Roughness estimator (radius > 20cm) ? Cloud Compare's EDL shading is very smooth, too smooth perhaps to show your point. Roughness with a single appropiate colour ramp for all 3 figures should demonstrate your need (along histogram of rpoughness values to objectivate your statement?). Alternatively, you may want to compute normals at 10-cm radius and display them. 10- cm is the half wavelength of the floor artefacts (figure 9). The surface roughness will appear as very variable values.

Section 4.2 Densification quality Cloud Compare's Cloud2Cloud distance estimate is used. This only provides a one-sided (absolute value) distance. Why not use M3C2 to provide a VLP16 to Zeb-Revo signed distance? What is the quality of the scan with Zeb-Revo?

> Figure 5 has been improved according to your suggestions. This is correct, the M3C2 tool from Cloudcompare has been used in the revised version. The accuracy announced by the Zeb-Revo is 1-3cm

Table 5 and table 6: what are the units of alpha-1 and alpha-2 ?

> These are angles and are expressed in degrees.

Section 5.3 line 211 "... with the Geolsam superposition +/- 2cm is present": what does it mean?

> This is the average distance between the two scans measured with the

Cloud2Cloud distance tool of Cloudcompare. This has been clarified.

line 212 "...presence of people in the scan" Why didn't you remove these points before collating the statistics. They are irrelevant for describing scanning quality. line 2018 "The wave frequency...", do you mean wavelength?

It's considered outliers. It has been removed in the revised version.

Sectiton 5.4 Origin of the short range artefacts Have you tried to check the ground pattern from a single beam? Glennie et al 2016 show that there are ranging inconsistencies in some beams of the VLP16 they tested. Their most external beams were range-biased. Could these defects explain the pattern you guys observe? Or else, is the tripod sufficiently rigid? Is there a ranging error dependant on a non-steady time constant?

The hypotheses put forward by the reviewer have already been verified. The waves are still present despite testing all of them, and their frequency are independent of the hardware setting, even when considering each beam separately.

Section 6 conclusions line 227: "The results ... are satisfactory" How so? There is no mission statement to argue about the acceptable nature of the result. You should state what acceptable means for your applications and perhaps reflect on a few applications which would be satisfied with this level of precision and this tool.

In our opinion, satisfactory means that the system has a sufficient level of accuracy for application in geoscience. The limit of acceptability has been better defined in the revised version.

line 229 "... verified the quality of registration". Registration of what? Wording ambiguous

In this context, it is the assembly of different scans (using an ICP algorithm). This has been clarified in the revised version.

Track changes

Dense point cloud acquisition with a low-cost Velodyne VLP-16

Jason Bula[1], Marc-Henri Derron[2], and Gregoire Mariethoz[1]

[1]University of Lausanne, Institute of Earth Surface Dynamics
[1]University of Lausanne, Institute of Earth Sciences

Abstract. This study develops a low-cost terrestrial lidar system (TLS) for dense point cloud acquisition. Our system consists of a VLP-16 lidar scanner produced by Velodyne which we have placed on a motorized rotating platform. This allows to continuously change the direction and densify the scan. Axis correction is performed in post-processing to obtain accurate scans. The system has been compared indoors with a high-cost system, showing an average absolute difference of $\pm$ 2.5 cm. Stability tests demonstrated an average distance of $\pm$ 2 cm between repeated scans with our system. The system has been tested in abandoned mines with promising results. It has a very low price (approximately 4000 dollars) and opens the door to measuring risky sectors where instrument loss is high but information valuable.

1 Introduction

These last decades, remote sensing and associated technologies have been developed and used to greatly improve environmental modelling. In particular, Light Detection and Ranging (hereafter lidar) has been proposed as a tool in geomatics to address such environmental modelling. Lidar technology is based on the Time of Flight (ToF, i.e. the time required by the light emitted by the laser to be reflected and captured again by the system) to measure distances. Lidar is useful for solving many problems. They are therefore widely used in geosciences, in particular for the management and the monitoring of environmental risks such as landslides, rock falls or cavity collapse (Lim et al., 2005 ; Teza et al., 2007 ; Jaboyedoff et al., 2011, Brideau et al., 2012; Royán et al., 2014; Michoud et al., 2015). The reliability of these measuring instruments is well established, but the technology is typically very expensive, which limits the potential applications of such systems.

New lidar-based obstacle avoidance technologies have been under development since the advent of autonomous cars. These mass-produced sensors are cheap but were not initially designed produce dense point clouds, and therefore have reduced ranges and resolutions. These low-cost systems have led to the development of new scanner systems that can be applied for mapping, especially for mobile terrestrial slam-based systems (James and Quinton., 2014 ; Dewez et al., 2017) or UAV slam-based system (Laurent et al,. 2019 ; Li et al,. 2014) and often requires the addition of an inertial station and Global Navigation Satellite System (GNSS).

Instruments used in geodesy such as theodolites or total stations must be calibrated to avoid measurement errors. This principle is also applied to lidar, which is constructed in a similar way. Lidar system calibration is a much studied subject in research. The aim is to determine the parameters that allow systematic errors to be reduced as much as possible. According to Neitzel 2006, three major errors may be present and are respectively : tilting axis error, collimation error, and eccentricity of

the line of sight. Some authors describe up to 21 possible calibration parameters (Lichti., 2007). There are different strategies for calibrating a lidar system. Research proposes a self-calibration based on mathematical models and by making geometric primitives as reference planes (Glennie and Lichti., 2010 ; Lerma and Garcia-San-Miguel 2014) or reference points (Neizel, 2006 ; Kesten et al., 2005). Other authors present calibration methods based on the use of a camera (Amiri Parian and Grün,. 2005 ; Lichti et al,. 2007).

Our study is based on the use of a low-cost lidar system which is the VLP-16 of Velodyne to elaborate of a low-cost TLS. This scanner currently, sold for 4000 dollars, has 16 parallel scan lines in a vertical field of view of $\pm$ 15 degrees, and a 360-degree horizontal scan plane (Figure 2c).Our idea was based on the addition of a rotating plate (which is a principle similar to that of many lidar systems) to produce a dense point cloud. Such a system particularly targets applications in rough field conditions, such as for example caves that are difficult to access. In such places there is the likelihood of damage to the equipment due to shocks, water, or dirt, which prevents the use of high-cost equipment. This type of system could also facilitate risk management in mines for the development of cave collapse risk maps, for example. The advantage is that the system is inexpensive, making it particularly suitable for permanent laser scanning in hazardous areas as described in (Williams et al., 2018). In addition, the power consumption of low-cost lidars is often very small, which is suitable for such environments.

The structure of this paper is as follows : section 2 presents the equipment and the constraints associated with it to produce a low-cost system. Section 3 presents the methodology used to produce high-resolution scans. Section 4 presents the result of our system. Section 5 discusses the results and section 6 presents some conclusions.

2   Low-cost hardware

2.1   VLP-16 Lidar

The VLP-16 model has 16 lasers fixed on a rotational head. The main features of the low-cost lidar can be found in table 1.

Table 1. Velodyne VLP-16

Channel	16
Wavelength	903 nm
Ranging accuracy	±3 cm (Typical)
Measurement Range	Up to 100m
Single Return Data Points	300000 pts/s
Maximum number of returns	2
Field of View (vertical)	30°
Vertical angular resolution	2.0°
Field of View (Horizontal)	360°
Horizontal angular resolution	0.1° − 0.4°
Laser rotation	10 Hz
Weight	830 g
Dimension	Ø 103mm, H 72mm
Retail Price	$4000

Each of the 16 parallel scan lines records up to 1875 points every tenth of a second, which corresponds to an angular horizontal resolution of 0.2 ° for a field of view of 360-degrees. Regarding the vertical resolution, the sensor is limited to a field of view of 30 degrees (Figure 2c). The 16 scan lines imply a low vertical angular resolution of 2.0°. Each of the 16 lasers in VLP-16 is individually aimed and, thus, each has a unique set of adjustment parameters. The mathematical model of VLP-16 which calculates the (x,y,z) coordinates is given in (Glennie et Lichti, 2010) as :

$$
\begin{bmatrix} x \\ y \\ z \end{bmatrix} = \begin{bmatrix} (s^i * R_i + D_o^i) * cos(\delta_i) * [sin(\varepsilon) * cos(\beta_i) - cos(\varepsilon_i)] - H_o^i * [cos(\varepsilon) * cos(\beta_i) + sin(\varepsilon) * sin(\beta_i)] \\ (s^i * R_i + D_o^i) * cos(\delta_i) * [cos(\varepsilon) * cos(\beta_i) + sin(\varepsilon_i)] + H_o^i * [sin(\varepsilon) * cos(\beta_i) - cos(\varepsilon) * sin(\beta_i)] \\ (s^i * R_i + D_o^i) * sin(\delta_i) + V_o^i \end{bmatrix}
$$

Where:

s^i is the distance scale factor for laser i;

D_o^i Do is the distance offset for laser i;

δ_i is the vertical rotation correction for laser i;

β_i is the horizontal rotation correction for laser i;

H_o^i is the horizontal offset from scanner frame origin for laser i;

V_o^i is the vertical offset from scanner frame origin for laser i;

R_i is the raw distance measurement from laser i;

ε is the encoder angle measurement.

The first six parameters are used to calibrate the system and can be found in the lidar data sheet. R_i and ε come from data collected during a measurement.

60   Figure 1a shows a photograph of the scanned scene with the same viewing angle, and Figure 1b shows a typical point cloud produced by the VLP-16 with highlighted vertical and horizontal angular resolutions. The poor vertical resolution limits the use of the VLP-16 for terrestrial scanning applications. For example, the low point density makes it difficult to co-register several scans.

2.2   Syrp Genie

65   With the purpose to have a low-cost design, we select the Syrp Genie Mini (table 2). This motorized head can rotate 360-degrees and sustain the weight of the lidar.

Table 2. Syrp Genie

Max rotation speed	0.58 rpm (35 s for 360-degrees)
Min rotation speed	0.0025 rpm
Payload	4 kg
Hardware Interface	Bluetooth 4.0
Dimensions	91.5 x 91.5 x 46mm
Retail Price	$250
Minimum step	0.005 degree

2.3   Conception and assembly of the custom scanning system

The VLP 16 is mounted on the Syrp Genie Mini, and the entire assembly is set on a photographic tripod and connected to a computer and a power source (Figure 2a). Importantly, the lidar is placed vertically using an L-shaped piece, such that the

70   vertical (low-resolution) and horizontal (high-resolution) directions are now reversed. It is also important to note that the term "vertical" corresponds to the lidar reference system and not necessarily to the direction of the gravitational field. Our goal is to use the slow rotating motion induced by the Syrp Genie Mini to densify the point cloud across the horizontal direction. It includes a stepper motor with a minimum step of 0.005 degree which does not impact the acquisition frequency of the VLP-16. A counterweight is placed on the tripod on the opposite side of the lidar to minimize stresses that can impact the rotation speed

75   and induce an angular distortion.

a)

b)

1) Horizontal angular resolution: 0.1º – 0.4º
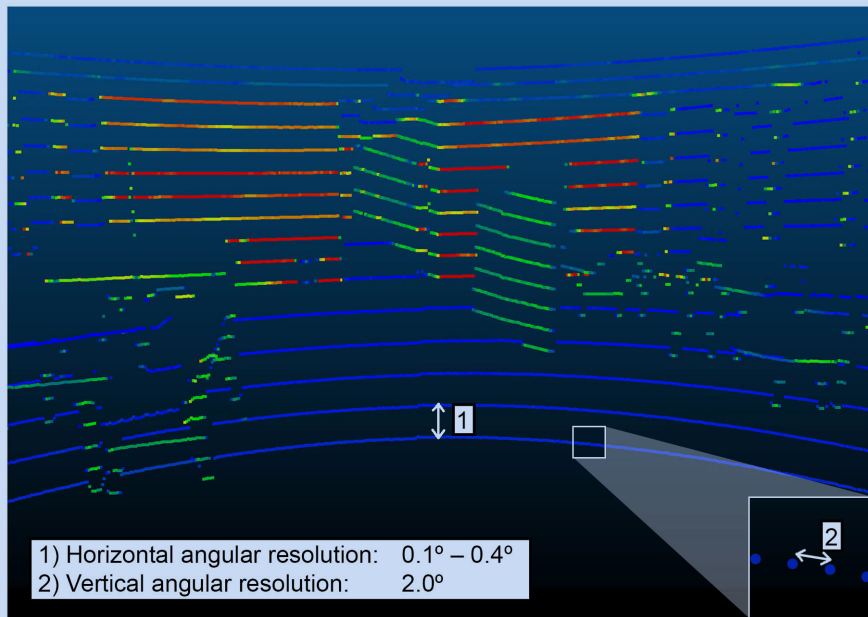2) Vertical angular resolution: 2.0º

Figure 1. (a) Picture of the scanned scene; (b) a typical scan created with the VLP-16, the color represents the intensity of the returned signal.
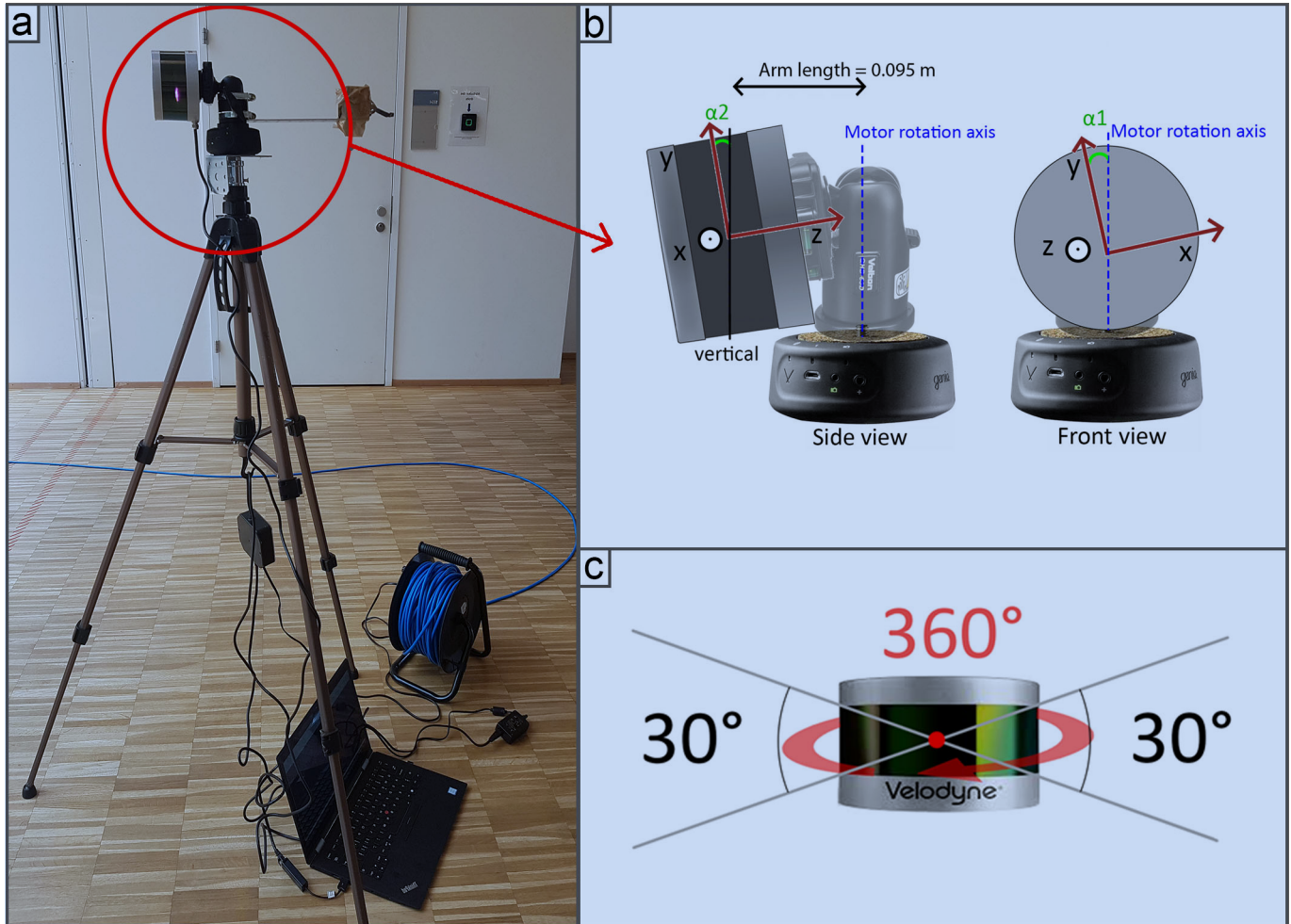
Figure 2. (a) Terrestrial lidar system (TLS); (b) two adjustments angles : collimation axis (α_1) and tilting axis (α_2) between the system and the rotation axis; (c) field of view of the VLP-16

3 Methodology

3.1 Data acquisition operation

Acquisition with our system requires a number of post-processing steps to obtain a scan that correctly represents the scene. For each acquisition, a 360-degree rotation is required to reconstruct a dense and accurate point cloud, the reason for this will be clarified in chapter 3.2. In order to ensure that the system does not record the acceleration and deceleration of the motor at the beginning and end of the rotation, the scans are made for a rotation of more than 360-degrees, which allows a better synchronization with the VLP-16. Once the engine starts its rotation, the scan is then started. The post-processing of the data consists in using the set of points (hereafter frame) produced at each rotation of the laser (10 rotations per second) and applying to it a transformation in relation to the motor speed. Figure 3 takes the example of a teapot to illustrate densification process, with 5 steps described below:

1. Frame at time $t = t_0$: Only a part of the teapot is scanned, corresponding to the lidar field of view (30 degrees). This first frame is used as reference to align the others.

2. Scan at time $t = t_1$: a second part of the teapot is scanned.

3. Representation of the scene when both frames are visible simultaneously. It is necessary to apply a transformation to correctly align both frames. This transformation is equal to a rotation on the y axis in clockwise direction by an angle corresponding to the rotation of the motor between t_0 and t_1.

4. Reconstructed scene after transformation: both frames are now aligned. Frames are incrementally assembled to construct the entire scene.

5. Visualization of the assemblage of frames acquired between time t_0 and t_f.

Assuming a constant geometry of the system, we use a rigid transformation between each frame. This geometrical transformation is characterized by a 4 x 4 matrix

$$T = \begin{bmatrix} a & b & c & 0 \\ d & e & f & 0 \\ g & h & i & 0 \\ j & k & l & 1 \end{bmatrix},$$

with:

- abc, the rotation applied on the x-axis
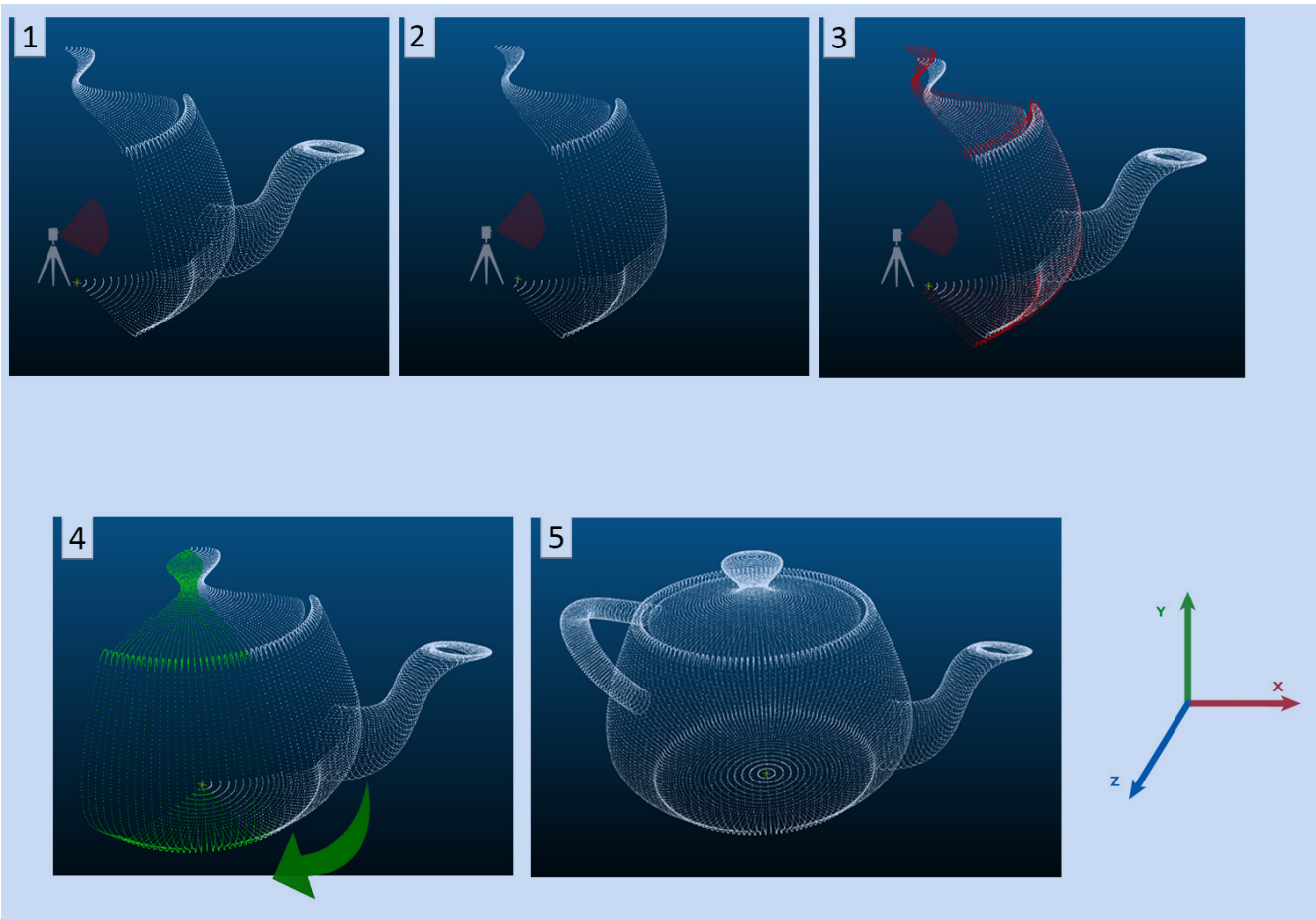
- def the rotation applied on the y-axis,

7

Figure 3. Steps to align the final. This is synthetic example assuming that the lidar is located in the center of the teapot point cloud

  – ghi the rotation applied on the z axis.

  – jkl the translation applied on x, y and z.

In our case, the rotation is applied around the y-axis, the transformation matrix that aligns each frame is equal to:

$$R = \begin{bmatrix} (cos(\beta) & 0 & sin(\beta) & 0 \\ 0 & 1 & 0 & 0 \\ -sin(\beta) & 0 & cos(\beta) & 0 \\ 0 & 0 & 0 & 1 \end{bmatrix},$$

with β the angle of the motor, which depends on the time since the start of the scan and the rotation speed. Once all frames are assembled, the entire point cloud can be visualized.

8

As the VLP-16 Puck has the particularity of being able to scan continuously and at 360-degrees, two sets of symmetrical point clouds representing respectively the points with positive and negative coordinates on the x-axis of the lidar reference frame (see Figure 5a) are created, which are theoretically superposed. This observation is a crucial point of the study as it allows the adjustment of the system in order to maximize this superposition (the adjustment procedure is described in section 3.2).

3.2 Post-processing and data adjustment

Since our system is custom-assembled, there is little control on exact mounting angles, which therefore require adjustments. Thus far, we have supposed that the system is turning around a fixed point corresponding to its optical center. In fact, given that the lidar is positioned on a ball head and a L-shaped piece, it is shifted from the rotation axis. This distance was measured using an electronic caliper and is equal to 0.095 m, for each frame a translation on the z axis was applied. The affine transformation is a matrix presented as follows:

$$T_2 = \begin{bmatrix} 1 & 0 & 0 & 0 \\ 0 & 1 & 0 & 0 \\ 0 & 0 & 1 & 0 \\ 0 & 0 & 0.095 & 1 \end{bmatrix}$$

Another important consideration is the correction to minimize systematic errors. Figure 2b shows two major adjustment parameters described in Neitzel 2006: α_1 for the collimation axis adjustment and α_2 for the tilting axis adjustment. . The manual adjustment of those two systems involves an offset that highly influence the point cloud geometry if uncorrected. As these offsets cannot be measured manually, an automatic adjustment is performed in post-processing.

To determine α_1 and α_2, the Nelder-Mead optimization algorithm is used, which is based on minimizing a continuous function using a simplex of dimensions equivalent to the number of parameters (Lagarias et al., 1998). At each iteration, a point located near the initial simplex is generated involving a new sample if a minimum is found, until convergence. The resolution of the densified scan is not regular. Indeed the point cloud resolution is very high near the lidar scanner and decreases away from the sensor. Because the algorithms for measuring the distance between two sets of point clouds require a lot of computer resources and must be repeated at each iteration of the Nelder-Mead optimization, the scans are downsampled using a grid average method to an uniform resolution. In addition, the optimization is carried out only for points within the distance range in the best accuracy range of 3 to 7 meters (Glennie et al., 2016).

The optimization seeks to obtain the α_1 and α_2 angles that minimize two functions:

1. During the rotation of the motor, the entire scene is recreated for each of the 16 scan lines. These identical scans are then put back together to form a dense point cloud. The overlap of the scans is influenced by changing the angle α_1 . Thus, the function to optimize corresponds to minimizing the average distance between the 16 full scenes that are superimposed.

2. The second function determines the angle α_2 based on the observation that both sets of symmetrical point clouds produced during the rotation must be exactly superposed. The variation of the angle α_2 creates a doming effect that tends to increase the average distance between both symmetrical point clouds (Figure 5a). α_2 is determined by minimizing this distance.

3.3 Effect of the adjustments and performance of the system

Visually, a wrong adjustment of α_1 results in blur around the scanned scene. A wrong adjustment of the α_2 angle results in a doming effect that increases away from the center. To illustrate this, several scans were carried out in a building of the University of Lausanne. A corridor of dimension 23 by 1.5 meters was scanned and a plane was fitted on the floor surface, which is supposed to be horizontal. This plane is based on a distance interval to the lidar equivalent to the best accuracy range, i.e. between 3 and 7 meters depending on the lidar performance tests (Glennie et al., 2016). This avoids the influence of points too close or too far away, which can distort the theoretical equation of the plane. In addition, the points selected for fitting the plane come from an adequate sub-sampling of the initial scan in order to standardize the density of points over the distance interval. Then, the distance of all points to this theoretical plane is evaluated, which gives an indication of the distribution of errors. Evaluation of the error as a function of the scanning distance was also measured.

Finally, reproducibility tests were performed to evaluate the stability of the system. To this end, the same scene was scanned 8 times in a row. The α_1 and α_2 parameters were then estimated separately. As the system is not transported or disassembled between measurements, the aim of this test was to evaluate the stability of these parameters. The average distance between each of the 8 scans is also evaluated using the M3C2 plugin of Cloudcompare with its default settings, which allows to compute signed (and robust) distances directly between two point clouds.

3.4 Testing the system in different environments

The system has been tested in various environments. For all scans performed, the Syrp Genie Mini has been configured to rotate 360-degrees in 6 minutes. These parameters allowed the acquisition of high point resolution to maximize the information collected while maintaining a reasonable scan time. With this setting, about 10 millions points per scan are collected. The first tests were carried out in a building of the University of Lausanne is characterized by vast surfaces and volumes. Then, the system was then used in a confined environment with no available GNSS signal: the Baulmes mines, a limestone mine disaffected at the end of the Second World War.

In these environments, several scans were assembled using the iterative closest point (ICP) alignment algorithm (Besl, P. J., McKay in 1992). This is the most popular method alignment approach for point clouds, which searches for nearest neighbors to minimize the distance between two point clouds.

3.5 Comparison with a high-cost system and field measurements

Our low-cost terrestrial lidar system was then compared to two other systems that fall into the high-cost category. These lidar systems are the Ilris 3D Optec and the Geoslam ZEB-REVO (table 3). The tests were carried out indoors and included one

measurement for each system. First, Figure 5 displays a picture of the scanned scene. As shown, objects were placed on the scene so that validation measurements could be taken with a tape measure in addition to the width and length of the corridor and the height of the ceiling. These distances were then measured for the scans coming from all three terrestrial lidar systems and compared to the measurements taken by hand. The different scans were also superimposed with an ICP algorithm to evaluate the average distance between the point clouds.
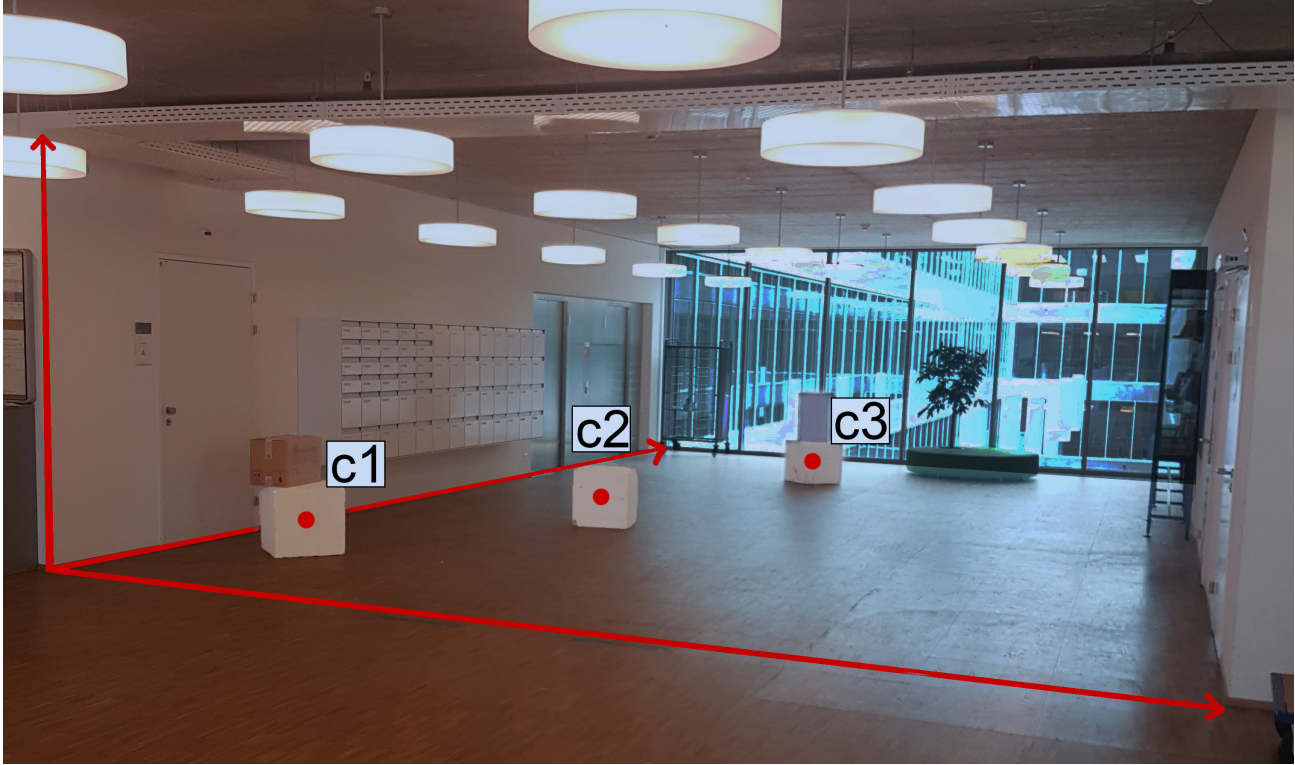

Figure 4. Picture of the scanned scene for lidar and distances comparison

Table 3. Main characteristics of lidar used

Parameter	Ilris-3D	Geoslam ZEB-REVO
Range	1200 m	30 m
Field of view	40 x 40 degrees	270 x 360-degrees
Ranging accuracy	7 mm @ 100 m	1 - 3 cm
Laser wavelength	1535 nm	905 nm
laser acquisition rate	2500 - 3500 points/sec	43.200 points/sec

4 Results

All point clouds are visualized in the CloudCompare software. An EDL (Eye Dome lighting) shading filter allowing the creation of real-time shading has been applied for better visualization (CloudCompare, 2019).
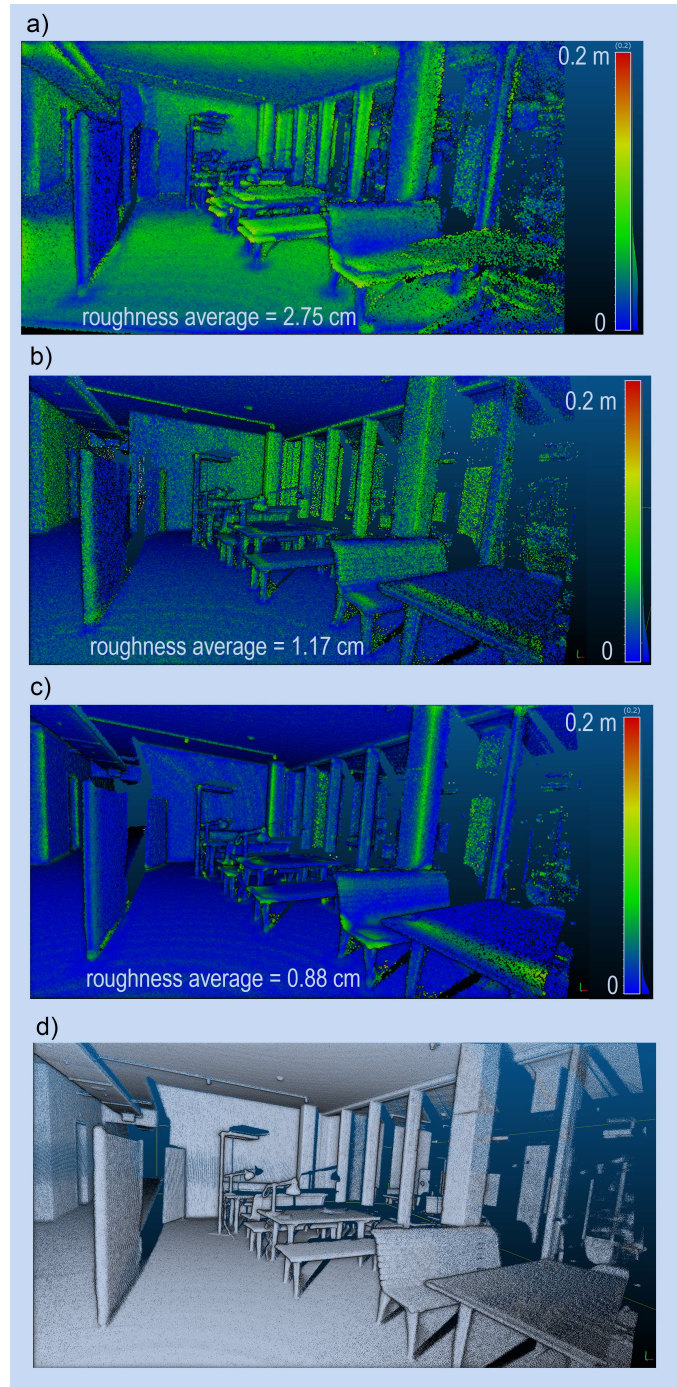
4.1 Effects of adjustments

Figure 5. Point cloud roughness for adjustment steps : (a) Scan without adjustments; (b) Scan after adjustments of α_1 and α_2, ; (c) final scan; (d) final scan (EDL filter)

Figure 5 shows the result of a scan that was carried out indoors in a work area of the University of Lausanne. Figure 5a shows the scene after the alignment of the different frames produced by the VLP-16 during the scan. A kind of blur caused by the splitting of the scene is observed. No processing has yet been applied, so the parameters α_1 and α_2 are set to 0. The color scale represents the roughness of the point cloud (for a radius of 0.2 m). Figure 5b shows the scene after adjusting the α_1 and α_2 parameters. The average roughness is equal to 1.17 cm. Figure 5c shows the scene where only the scanned points corresponding to the positive coordinates on the x-axis are displayed (i.e., 50% of the data are discarded). In addition, a sub-sampling at 0.005m is applied using a grid average method and a statistical outlier removal is performed in cloudCompare. The average roughness is equal to 0.88 cm. Figure 5d is a copy of 5c with an Eye-dome-lighting filter.

Figure 6 shows the error corresponding to the distance of the points from the theoretical plane and the error histogram for the three adjustments steps respectively.
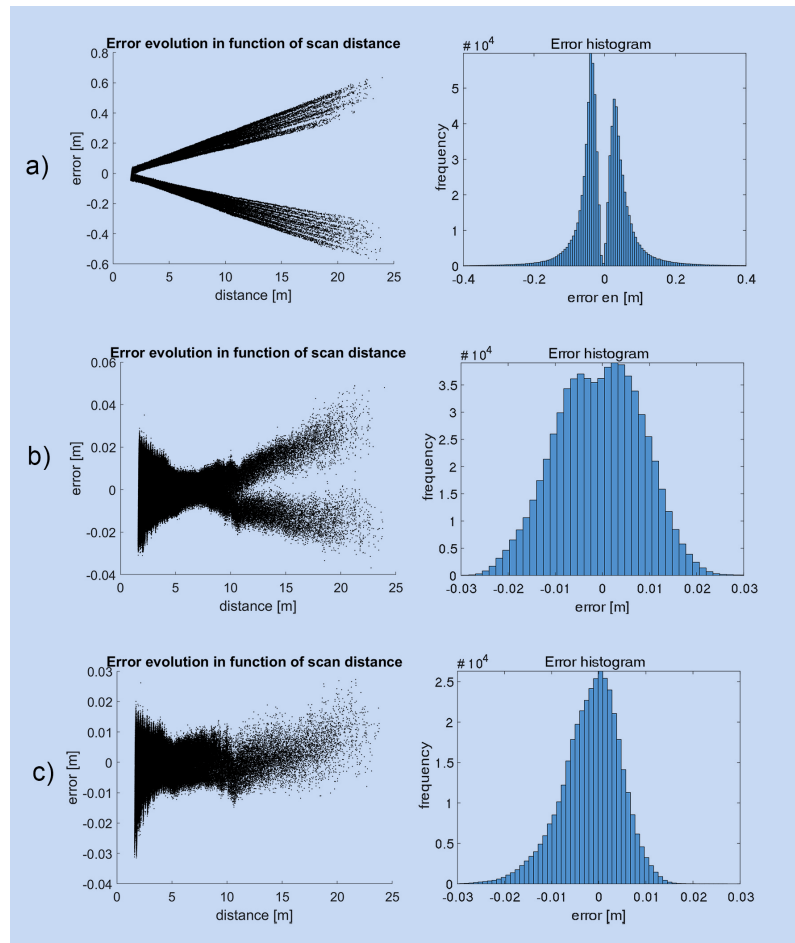

Figure 6. Effects of adjustments in relation to a theoretical plane : (a) Error estimation before calibration; (b) Error estimation after adjustments; (c) Error estimation after post-treatment

4.2 Overview of the densification quality

Figure 7a provides an overview of a scan performed indoors after adjustments. A photograph of the scanned scene with the same viewing angle is shown in Figure 7b. Note the improvement compared to Figure 1 where the VLP-16 was used alone.

Figures 8a and 8b show two previews of scans performed at the Baulmes mines.

190   Figure 8c shows the result of the registration of 4 point clouds in the Baulmes mines. The points corresponding to each of the acquisitions are represented in a different color to highlight the registration. It should be noted that the clouds have not been cleaned to removed outliers, so we can see that the sensor has scanned itself. The results are characterized by a spacing set at 0.005 meters and is visually realistic.
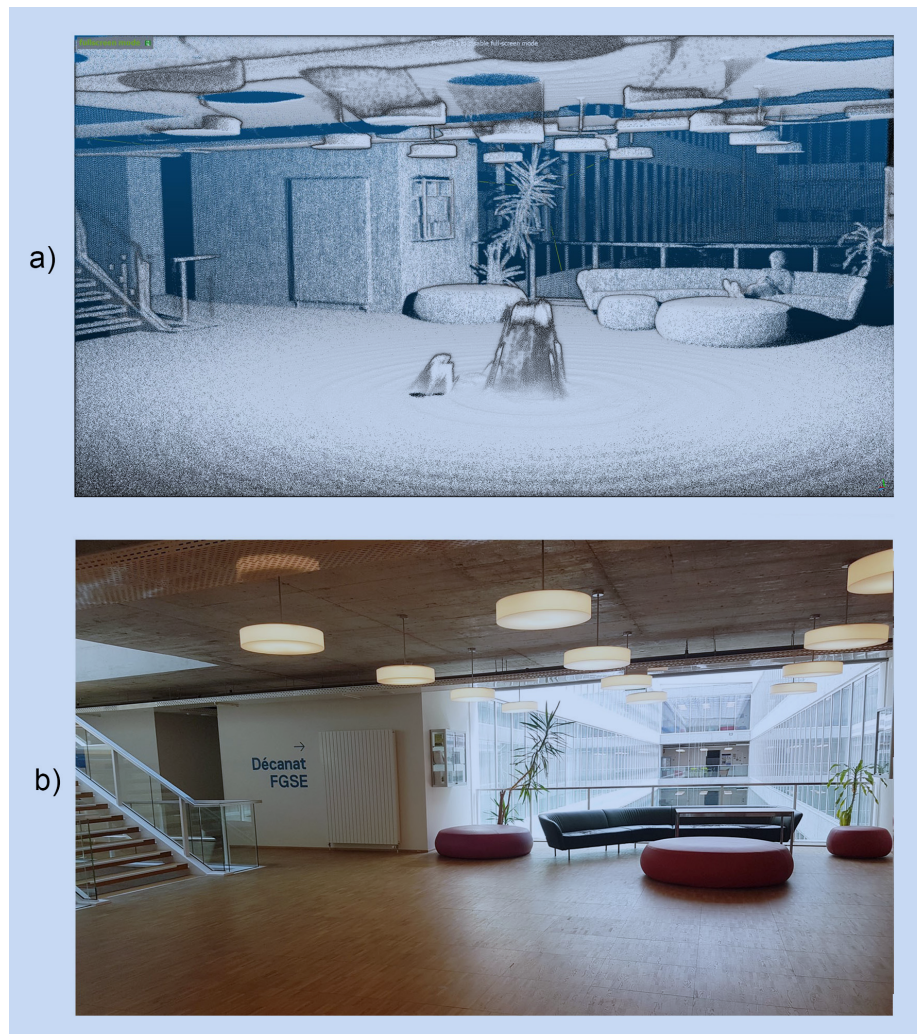

Figure 7. Example of point cloud densification after adjustments of the system : (a) Result of an indoor point cloud densification; (b) Picture of the scene
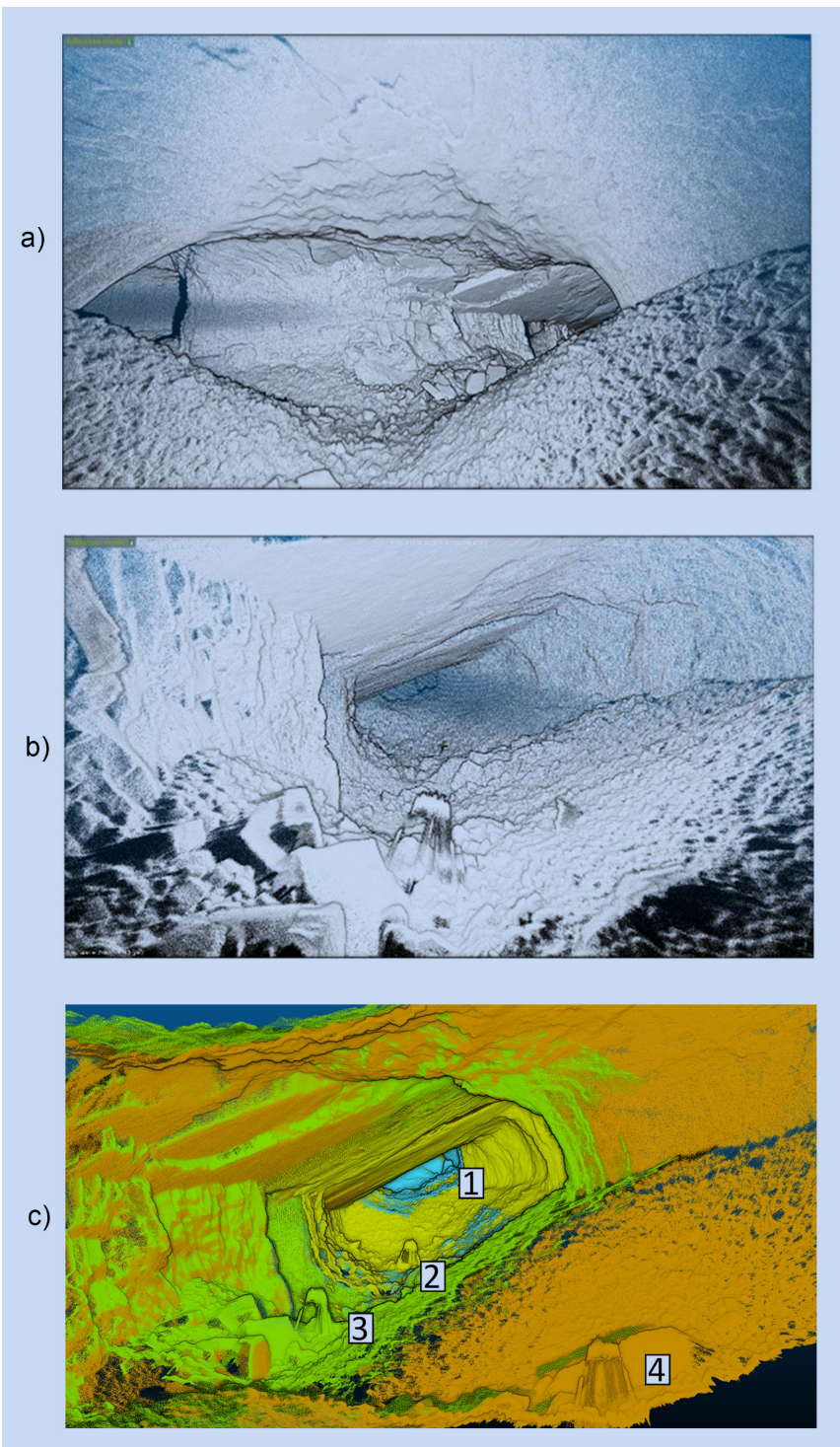
Figure 8. Scanned scenes in Baulmes mines. The height of the gallery is about 3.5 m : (a) Mine example 1; (b) Mine example 2; (c) Point cloud registration in the mine

4.3 Data analysis and validation

195 During the visualization of the point clouds, we observed the presence of an artifact on all of our measurements. Figure 9 illustrates this artifact, which is characterized by wavelets near the system that fade away with distance.
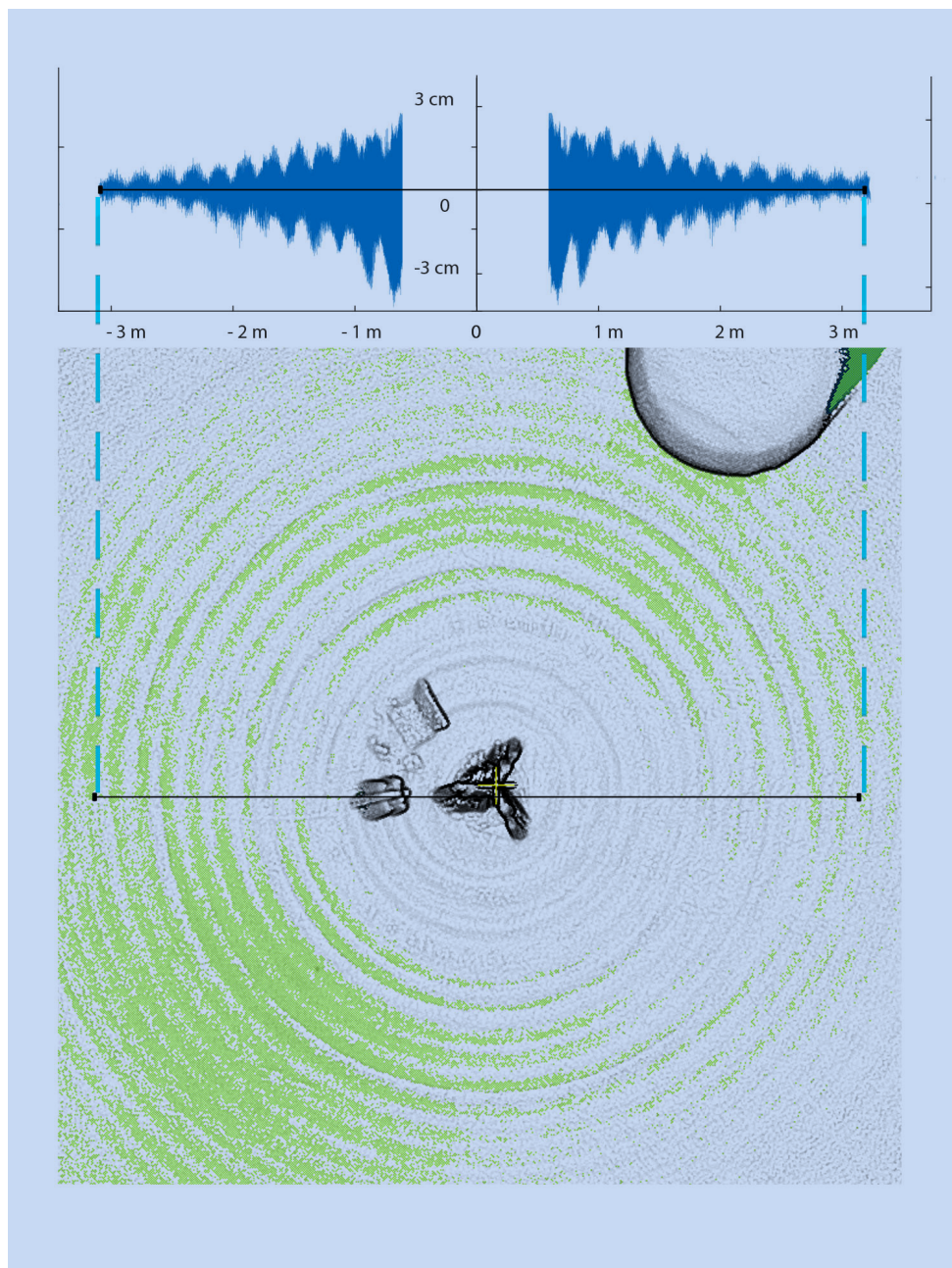

Figure 9. Artifact present near the TLS and its corresponding amplitude

Table 4 shows the ability of the system to reproduce the same point cloud by comparing 8 consecutive measurements. Each of these measurements is compared to the other 7 by measuring the average distance between pairs of scans (in meters). Table 5 shows the variation of the parameters α_1 and α_2 during this reproducibility test. Table 6 summarizes the different measurements made with the VLP-16, Ilris-3D and Geoslam. The data are also compared with manual measurements.

Table 4. Distance between all of the 8 scans of the reproductibility test

Scan number	1	2	3	4	5	6	7	8
1	0.000	0.014	0.019	0.018	0.020	0.021	0.022	0.016
2		0.000	0.019	0.019	0.020	0.022	0.021	0.016
3			0.000	0.013	0.015	0.016	0.016	0.019
4				0.000	0.014	0.016	0.016	0.019
5					0.000	0.015	0.015	0.020
6						0.000	0.015	0.022
7							0.000	0.021
8								0.000

Table 5. Variability of α_1 and α_2 parameters during reproducibility test

Num.	α_1 [degre]	α_2 [degre]
1	0.40	-0.00
2	0.40	-0.01
3	0.09	-0.03
4	0.11	-0.04
5	0.05	0.00
6	0.05	0.00
7	0.07	0.02
8	0.34	-0.09

Table 6. Comparison of field and lidar measurements

	Field [m]	VLP [m]	Ilris [m]	Geoslam [m]
Ceiling	3.005	3.001	3.003	2.964
Length	11.945	11.932	11.970	11.931
Width	7.145	7.127	7.117	7.087
Cube dimension	0.500	0.500	0.498	0.509
c1 -c2	2.715	2.730	2.719	2.741
c2 - c3	4.635	4.645	4.625	4.832
c1 - c3	7.545	7.519	7.478	7.473
ABS Mean difference	Field [m]	0	0.0123	0.0197	0.0596

To validate the registration, the comparison of the distances between the points coming from our assembly and those coming from GeoSLAM was carried out using CloudCompare with the option "Cloud to cloud distance". The average distance between both point clouds and the standard deviations of these distances are shown in Table 4.

Table 7. Mean distance between Ilris, Geoslam and Velodyne TLS (M3C2 distance)

	Mean distance [m]
Optec Ilris vs. VLP-16 TLS	± 0.025
Optec Ilris vs. Geoslam	± 0.067
VLP-16 TLS vs Geoslam	± 0.051

5. Discussion

205 ### 5.1 Data analysis before and after adjustment

As shown in Figure 5, adjustment is a fundamental step in producing accurate 3D modeling of an environment.

The use of the two symmetrical datasets produced during an acquisition using the VLP-16 is a key element in the optimization of the system. However, as shown in Figure 5b, the roughness calculation tells us that the entire point cloud could silll be smoother. For this reason, we decided to keep only half of the points (Figure 5c and Figure 5d) in order to obtain a sharper

210 representation of the scene. This choice will be justified after the analysis of the following analysis.

The error depends on the distance to the lidar. Before adjustment, the distance to the theoretical plane varies from about $\pm$ 4 cm ($\mu \pm 1\,\sigma$) for the closest points to the lidar to 59 cm ($\mu \pm 1\,\sigma$) for a scan distance of 23 m (Figure 6a). After adjustment of parameters α_1 and α_2, the entire point cloud approaches the theoretical surface, as shown in Figure 6b. However the evolution

of the error as a function of distance is still not constant and tends to increase linearly with the scan distance. The minimum error is logically in the point range where the theoretical plane is situated. The bimodal error histogram shown in Figure 6b and (centered at $\pm$ 0.5 cm) shows that the superposition between the two halves of the scan is still not entirely accurate despite the adjustment performed.

The evolution of the error as a function of the scanning distance when keeping only one half of the scan (Figure 6c) shows an accuracy range of $\pm$ 2.5 cm ($\mu \pm 1.5\,\sigma$), which remains within the accuracy range given by Velodyne. The post-processing steps and the adjustment of mounting angles has allowed to drastically reduce errors; however, the adjustment parameters vary greatly between scans, as shown in table 5 and table 6. This can be explained by the assembly of our lidar system being relatively unstable. The impact of the adjustment, and particularly the need to repeat the adjustment for each scan, could be alleviated by welding together the different components of the system.

5.2 Performance and stability of the TLS

According to the manufacturer's website, the VLP-16 Puck allows data acquisition at a distance of 100 m for an accuracy of $\pm$ 3 cm, under optimal acquisition conditions. Various stability tests have been carried out in a metrology laboratory, which indicates an accuracy of $\pm$ 2 cm for an acquisition distance of 5 meters to a white and flat target (Glennie, et al., 2016). Reproducibility tests tell us that the system is quite stable when it is not moved or disassembled. The α_1 adjustment parameter shows a slight variation for scans 1, 2 and 8. This can be explained by the Nelder-Mead algorithm which finds a local and not a global minimum of the function.

The calculation of the average distance between all scans (table 4) indicates a small variation in the scanned scene. The measured distances are mostly below 2 cm, confirming the tests performed by Glennie, et al. 2016 and may be related to noise. We can see a correlation between scan pairs having similar adjustment parameters (scans 1, 2, 8) and their average distances.

5.3 Comparison with high-cost hardware and field measurements

The measurements taken manually in the field have enabled comparisons with the scans obtained with our system. Table 6 shows that the measurements taken with the VLP-16 TLS are closest to ground truth, with an average of 1.23 cm compared to 1.97 cm for the Optec and 5.96 cm for the Geoslam. This result should be taken with caution as it may be specific to our experimental setup. It should also be taken into account that a sub-sampling at 0.5 cm from the scans was performed using a grid average method.

After alignment using an ICP algorithm, the scans could be compared and are presented in Table 7. Assuming that the Optec system is the most accurate, our system achieves a good performance with an average distance of $\pm$ 2.5 cm. Geoslam obtains a lower level of accuracy with an average of $\pm$ 6.7 cm.

5.4 Origin of the short-range artifacts

Visually, this artifact is easily observed in the results of scans near the tripod,when data acquired on a flat surface. Figure 9 shows the influence of this artifact on the scan. We notice that the error spreads in the form of regular waves and fades away as it moves away from the lidar. It has a magnitude of 3 cm at the closest to the lidar and drops below 1.5 cm at a distance of 3 m. The wave frequency is about 20 cm. A hypothesis on the origin of this artifact would be related to the length of the arm which was measured manually. It turns out that errors in the length of the arm has no influence on the occurrence of these artifacts, but instead creates horizontal deformations. We also tested by using each laser separately, by using another tripod, and by varying the parameters and changing the motor speed. However, the artifacts remain constant (same distance and amplitude between waves). This indicates that the artifacts seem to be related to the lidar itself. Since the error appears to be regular, it would be conceivable to correct outliers by modifying each point according to the distance to the lidar.

6 Conclusion

This paper presents a low-cost terrestrial lidar system based on the use of a Velodyne VLP-16. Comparisons with high-precision models allow validating the accuracy of the system, which seems promising. As shown in the results, our system requires adjustment for each scan performed. These adjustments are made in post-processing and are possible thanks to the data acquisition geometry of the VLP-16. This could be avoided if the system components were welded together. However, we wanted to keep the possibility separating these elements in order to use the lidar for other projects, for example. The use of the lidar system in an underground mine demonstrates the potential applications of such a system in particular in the field of geosciences.

Code availability. Velodyne TLS

GitHUB repository

Data availability.

Code and data availability.

Sample availability.

Video supplement.

Baulmes

Reclere

Milandre

Rolex Learning Center

270 Appendix A

A1

References

Amiri Parian, J. and Grün, A.: Integrated laser scanner and intensity image calibration and accuracy assessment, in International Archives of
280   the Photogrammetry, Remote Sensing and Spatial Information Sciences, vol. 36, pp. 18–23, ISPRS., 2005.

Besl, P. J. and McKay, N. D.: Method for registration of 3-D shapes, in Sensor Fusion IV: Control Paradigms and Data Structures, vol. 1611,
pp. 586–606, International Society for Optics and Photonics., 1992.

Brideau, M.-A., Sturzenegger, M., Stead, D., Jaboyedoff, M., Lawrence, M., Roberts, N. J., Ward, B. C., Millard, T. H. and Clague, J.
J.: Stability analysis of the 2007 Chehalis lake landslide based on long-range terrestrial photogrammetry and airborne LiDAR data,
285   Landslides, 9(1), 75–91, doi:10.1007/s10346-011-0286-4, 2012.

Dewez, T. J. B., Yart, S., Thuon, Y., Pannet, P. and Plat, E.: Towards cavity-collapse hazard maps with Zeb-Revo handheld laser scanner
point clouds, The Photogrammetric Record, 32(160), 354–376, doi:10.1111/phor.12223, 2017.

Glennie, C. and Lichti, D. D. (2010). Static Calibration and Analysis of the Velodyne HDL-64E S2 for High Accuracy Mobile Scanning,
Remote Sensing, 2(6), 1610–1624, doi:10.3390/rs2061610, 2010.

290   Glennie, C. and Lichti, D. D.: Static Calibration and Analysis of the Velodyne HDL-64E S2 for High Accuracy Mobile Scanning, Remote
Sensing, 2(6), 1610–1624, doi:10.3390/rs2061610, 2010.

Glennie, C. L., Kusari, A. and Facchin, A.: Calibration and stability analysis of the VLP-16 laser scanner, Int. Arch. Photogramm. Remote
Sens. Spatial Inf. Sci., XL-3/W4, 55–60, doi:10.5194/isprs-archives-XL-3-W4-55-2016, 2016.

Jaboyedoff, M., Oppikofer, T., Abellán, A., Derron, M.-H., Loye, A., Metzger, R. and Pedrazzini, A.: Use of LIDAR in landslide investiga-
295   tions: a review, Nat Hazards, 61(1), 5–28, doi:10.1007/s11069-010-9634-2, 2012.

James, M. R. and Quinton, J. N.: Ultra-rapid topographic surveying for complex environments: the hand-held mobile laser scanner (HMLS):
ULTRA-RAPID TOPOGRAPHIC SURVEYING: THE HMLS, Earth Surf. Process. Landforms, 39(1), 138–142, doi:10.1002/esp.3489,
2014.

Kersten, Thomas Sternberg, Harald Mechelke, Klaus. (2005). Investigations into the accuracy behaviour of the terrestrial laser scanning
300   system Mensi GS100. Optical 3-D Measurement Techniques VII. 1. 122-131.

Lagarias, J. C., Reeds, J. A., Wright, M. H. and Wright, P. E.: Convergence Properties of the Nelder–Mead Simplex Method in Low Dimen-
sions, SIAM J. Optim., 9(1), 112–147, doi:10.1137/S1052623496303470, 1998.

Laurent, A., Moret, P., Fabre, J. M., Calastrenc, C., Poirier, N.: La cartographie multi-scalaire d'un habitat sur un site accidenté: la Silla del
Papa (Espagne), 2019.

305   Lerma, J. L. and García-San-Miguel, D.: Self-calibration of terrestrial laser scanners: selection of the best geometric additional parameters,
ISPRS Ann. Photogramm. Remote Sens. Spatial Inf. Sci., II–5, 219–226, doi:10.5194/isprsannals-II-5-219-2014, 2014.

Li, R., Liu, J., Zhang, L. and Hang, Y.: LIDAR/MEMS IMU integrated navigation (SLAM) method for a small UAV in indoor environments,
in 2014 DGON Inertial Sensors and Systems (ISS), pp. 1–15, IEEE, Karlsruhe, Germany., 2014.

Lichti, D. D.: Error modelling, calibration and analysis of an AM–CW terrestrial laser scanner system, ISPRS Journal of Photogrammetry
310   and Remote Sensing, 61(5), 307–324, doi:10.1016/j.isprsjprs.2006.10.004, 2007.

Lichti, D., Brustle, S., Franke, J. (2007). Self-calibration and analysis of the Surphaser 25HS 3D scanner. Proceedings of the Strategic
Integration of Surveying Services, FIG Working Week, Hong

Lim, M., Petley, D. N., Rosser, N. J., Allison, R. J., Long, A. J. and Pybus, D.: Combined Digital Photogrammetry and Time-of-Flight Laser
Scanning for Monitoring Cliff Evolution, The Photogrammetric Record, 20(110), 109–129, doi:10.1111/j.1477-9730.2005.00315.x, 2005.

315 Michoud, C., Carrea, D., Costa, S., Derron, M.-H., Jaboyedoff, M., Delacourt, C., Maquaire, O., Letortu, P. and Davidson, R.: Landslide detection and monitoring capability of boat-based mobile laser scanning along Dieppe coastal cliffs, Normandy, Landslides, 12(2), 403–418, doi:10.1007/s10346-014-0542-5, 2015.

Neitzel, F. (2006). Investigation of Axes Errors of Terrestrial Laser Scanners.

Northend, C. A., Honey, R. C. and Evans, W. E.: Laser Radar (Lidar) for Meteorological Observations, Review of Scientific Instruments, 37(4), 393–400, doi:10.1063/1.1720199, 1966.

320 Royán, M. J., Abellán, A., Jaboyedoff, M., Vilaplana, J. M. and Calvet, J.: Spatio-temporal analysis of rockfall pre-failure deformation using Terrestrial LiDAR, Landslides, 11(4), 697–709, doi:10.1007/s10346-013-0442-0, 2014.

Royán, M. J., Abellán, A., Jaboyedoff, M., Vilaplana, J. M. and Calvet, J.: Spatio-temporal analysis of rockfall pre-failure deformation using Terrestrial LiDAR, Landslides, 11(4), 697–709, doi:10.1007/s10346-013-0442-0, 2014.

325 Teza, G., Galgaro, A., Zaltron, N. and Genevois, R.: Terrestrial laser scanner to detect landslide displacement fields: a new approach, International Journal of Remote Sensing, 28(16), 3425–3446, doi:10.1080/01431160601024234, 2007.

Williams, J. G., Rosser, N. J., Hardy, R. J., Brain, M. J. and Afana, A. A.: Optimising 4-D surface change detection: an approach for capturing rockfall magnitude–frequency, Earth Surface Dynamics, 6(1), 101–119, doi:https://doi.org/10.5194/esurf-6-101-2018, 2018.

Response RC#1

Dense point cloud acquisition with a low-cost Velodyne VLP-16

Jason Bula[1], Marc-Henri Derron[2], and Gregoire Mariethoz[1]

[1]University of Lausanne, Institute of Earth Surface Dynamics
[1]University of Lausanne, Institute of Earth Sciences

Abstract. This study develops a method to acquire dense point clouds with a low-cost Velodyne VLP-16 lidar system, without using expensive GNSS positioning or IMU. Our setting consists in mounting the lidar on a motor to continuously change the scan direction, which leads to a significant increase in the point cloud density. A post-treatment reconstructs the position of each point accounting for the motor angle at the time of acquisition, and a calibration step accounts for inaccuracies in the

5   hardware assemblage. The system is tested in indoors settings such as buildings and abandoned mines, but is also expected to give good results outdoors. It is also compared with a more expensive system based on IMU registration and a SLAM algorithm. The alignment between acquisitions with those two systems is within a distance of 2 cm.

1   Introduction

In the last years, sensor enhancements and the development of new platforms have led to an increased use of 3D data acquisition

10   techniques. Lidar (light detection and ranging) is an active sensor that uses the principle of time of flight to measure the distance between the sensor and the intended target to produce a 3D point cloud. The first models were atmospheric lidars launched in the 1960s. Those were used to characterize clouds (Northend et al,. 1966; Davis, 1969) or to quantify of aerosols (Schuster, 1970). Afterwards, terrestrial lidars (TLS) have been developed to measure hard targets (Ackermann, 1999) for static or mobile systems and for high-resolution modeling. Common applications include civil engineering (Barnea et Filin, 2008), management

15   of environmental hazards like landslide or rock fall (Jaboyedoff et al., 2011, 2012; Royán et al., 2014; Teza et al., 2007), or the acquisition of topographic data (Shan et Toth, 2018).

Despite a clear potential, the use of lidar is often limited by the high cost of data acquisition. Over the last decade, low-cost lidars have been launched, but those models have generally limited performance compared to the high-cost lidars. New low-cost lidar generally use rotational mirror that increase the number of scanning line and thus measure more points per second

20   (Shakleton et al., 2010). Their range is generally less than 200 meters and the resolution of the resulting point clouds is low. However, these new systems often allow very high speed data acquisition comparable to high-cost devices. In addition, low-cost lidars are very compact and therefore quick to set up in the field. This makes them promising tools in terms of efficiency (Wang et al., 2018). Such low-cost sensors are mainly used for self-driving cars (Geiger et al., 2012) or for UAV-based surveys. They typically provide a level of accuracy of the order to 5-15 cm (Stöcker et al,. 2017; Laurent et al,. 2019). Low-cost lidars

25   are widely used in robotics for obstacle avoidance for instance, but more rarely for mapping because such systems do not produce dense point cloud.

1

The objective of this study is to develop a method to effectively use the data produced by a low-cost lidar (Velodyne VPL-16 which can scan continuously and takes 10 frames per second) in order to produce a dense point cloud while avoiding high-cost equipment. The idea of our approach is to continuously rotate the lidar along the axis of lowest beam density. With a slow

30 controlled rotating movement and a continuous acquisition mode, it is possible to densify the acquired point cloud such that it is comparable to data obtained with higher grade systems.

The structure of this paper is as follows : section 2 presents the equipment and the constraints associated with it to produce a low-cost system. Section 3 present the methodology used to produce high-resolution scans. Section 4 presents the result of our system. Section 5 discusses the results section 6 presents some conclusions.

35 ## 2 Low-cost hardware

2.1 VLP-16 Lidar

The VLP-16 model has several lasers fixed on a rotational head. The main features of the low-cost lidar can be found in table 1.

Table 1. Velodyne VLP-16

Channel	16
Wavelength	903 nm
Accuracy	±3 cm (Typical)
Measurement Range	Up to 100m
Single Return Data Points	300000 pts/s
Field of View (vertical)	30°
Angular Resolution (vertical)	2.0°
Field of View (Horizontal)	360°
Horizontal Angular Resolution	0.1° − 0.4°
Frame rate	10 fps
Weight	830 g
Dimension	Ø 103mm, H 72mm
Retail Price	$4000

Geoscientific
Instrumentation
Methods and
Data Systems
Discussions
Open Access
EGU

Table 2. Syrp Genie

Max rotation speed	0.58 rpm (35 s for 360 degrees)
Min rotation speed	0.0025 rpm
Payload	4 kg
Hardware Interface	Bluetooth 4.0
Dimensions	91.5 x 91.5 x 46mm
Retail Price	$250
Minimum step	0.005 degree

The acquisition mode of the VLP-16 consist in 16 fixed parallel scan lines. Each scan line records 1810 points per image, which corresponds to a angular horizontal resolution of 0.2 °. Regarding the vertical resolution, the sensor is limited to a field of view of 30 degrees. The 16 scan lines imply a low vertical angular resolution of 2.0°. Figure 1b shows a typical point cloud produced by the VLP-16 and figure 1a shows a photograph of the scanned scene with the same viewing angle. This poor resolution limits the use of the VLP-16 for terrestrial scanning applications. For example the low point density makes it difficult to co-register several scans

2.2 Syrp Genie

With the purpose to have a low-cost design, we select the Syrp Genie Mini (table 2). This motorized head can rotate 360 degrees and sustain the weight of the VLP-16.

2.3 Conception and assembly of the custom scanning system

The VLP 16 is mounted on the Syrp Genie Mini, and the entire assembly is set on an ordinary tripod and connected to a computer and a power source (figure 2). Importantly, the lidar is placed vertically using an L-shaped piece, such that the vertical (low-resolution) and horizontal (high-resolution) directions are now reversed. Our goal is to use the slow rotating motion induced by the Syrp Genie Mini to densify the point cloud across the horizontal direction. A counterweight is placed on the tripod on the opposite side of the lidar to minimize stresses that can impact the rotation speed and induce an angular distortions.

3 Methodology

3.1 Post-treatment of the data

Acquisition with our system requires a number of post-treatment steps to obtain a scan that correctly represents the scene. At the beginning of the scan, the rotation speed and the time lapse between the start and the stop of the rotation are recorded.
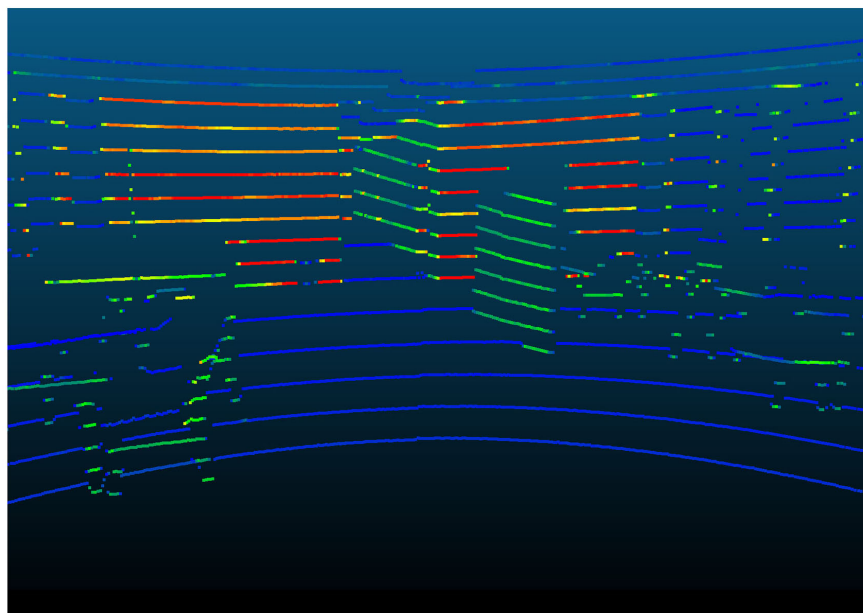
a)

b)

Figure 1. Typical scan created with the VLP-16, the color represents the intensity of the returned signal.

Figure 2. Terrestrial lidar system (TLS)

Then, each frame is rotated by the angle corresponding to the time of acquisition. Figure 3 takes the example of a teapot to
60   illustrate densification process, with 5 steps described below:

1. Frame at time $t = t_0$: Only a part of the teapot is scanned, corresponding to the lidar field of view (30 degrees). This
   first frame is used as reference to align the others.

2. Scan at time $t = t_1$: a second part of the teapot is scanned.

3. Representation of the scene when both frames are visible simultaneously. It is necessary to apply a transformation to
   correctly align both frames. This transformation is equal to a rotation on the y axis in clockwise direction by an angle
   corresponding to the rotation of the motor between t_0 and t_1.

4. Image after transformation: both frames are now aligned. Frames are incrementally assembled to construct the entire
   scene.

5. Visualization of the assemblage of frames acquired between time t_0 and t_f.

70

Assuming a constant geometry of the system, we use a rigid transformation between each frame. This geometrical transfor-
mation is characterized by a 4 x 4 matrix

$$T = \begin{bmatrix} a & b & c & 0 \\ d & e & f & 0 \\ g & h & i & 0 \\ j & k & l & 1 \end{bmatrix},$$

with:

- abc, the rotation applied on the x-axis

75   - def the rotation applied on the y-axis,

- ghi the rotation applied on the z axis.

- jkl the translation applied on x, y and z.

In our case, the rotation is applied around the y-axis, the transformation matrix that aligns each frame is equal to:

$$T_1 = \begin{bmatrix} (cos(\beta)) & 0 & sin(\beta) & 0 \\ 0 & 1 & 0 & 0 \\ -sin(\beta) & 0 & cos(\beta) & 0 \\ 0 & 0 & 0 & 1 \end{bmatrix},$$
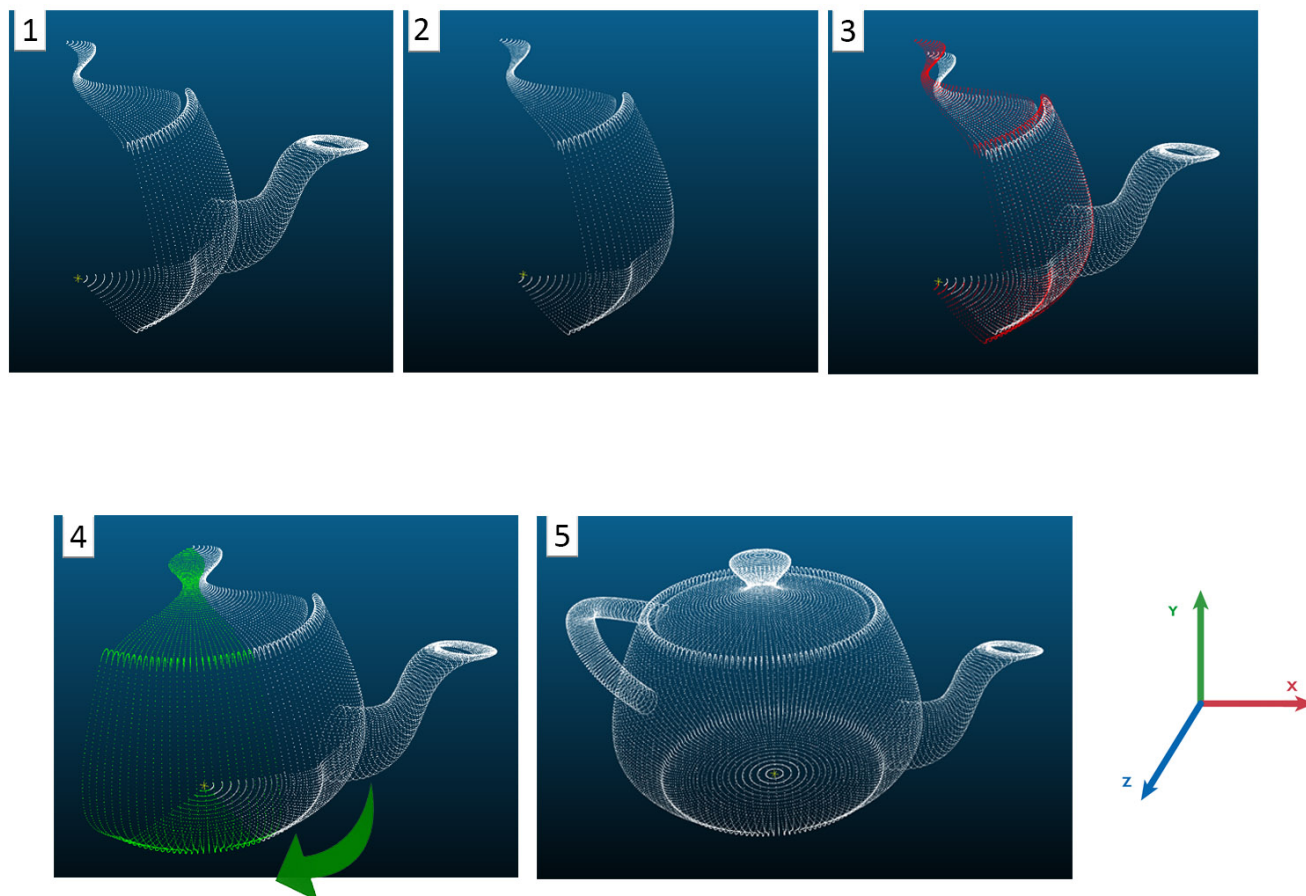
6

Geoscientific
Instrumentation
Methods and
Data Systems

Open Access

Discussions

EGU

Figure 3. Steps to align the final. This is synthetic example assuming that the lidar is located in the center of the teapot point cloud

with β the angle of the motor, which depends on the time since the start of the scan and the rotation speed. Once all frames are assembled, the entire point cloud can be visualized.

As the VLP-16 Puck has the particularity of being able to scan continuously and at 360 degrees, two sets of symmetrical point clouds representing respectively the points with positive and negative coordinates on the x-axis of the lidar reference frame (see figure 5a) are created, which are theoretically superposed. This observation is a crucial point of the study as it allows the calibrating of the system in order to maximize this superposition (the calibration procedure is described in section 3.2).

3.2 Calibration of the lidar system

Since our system is custom-assembled, there is little control on exact mounting angles, which therefore require calibration. Thus far, we have supposed that the system is turning around a fixed point corresponding to its optical center. In fact, given
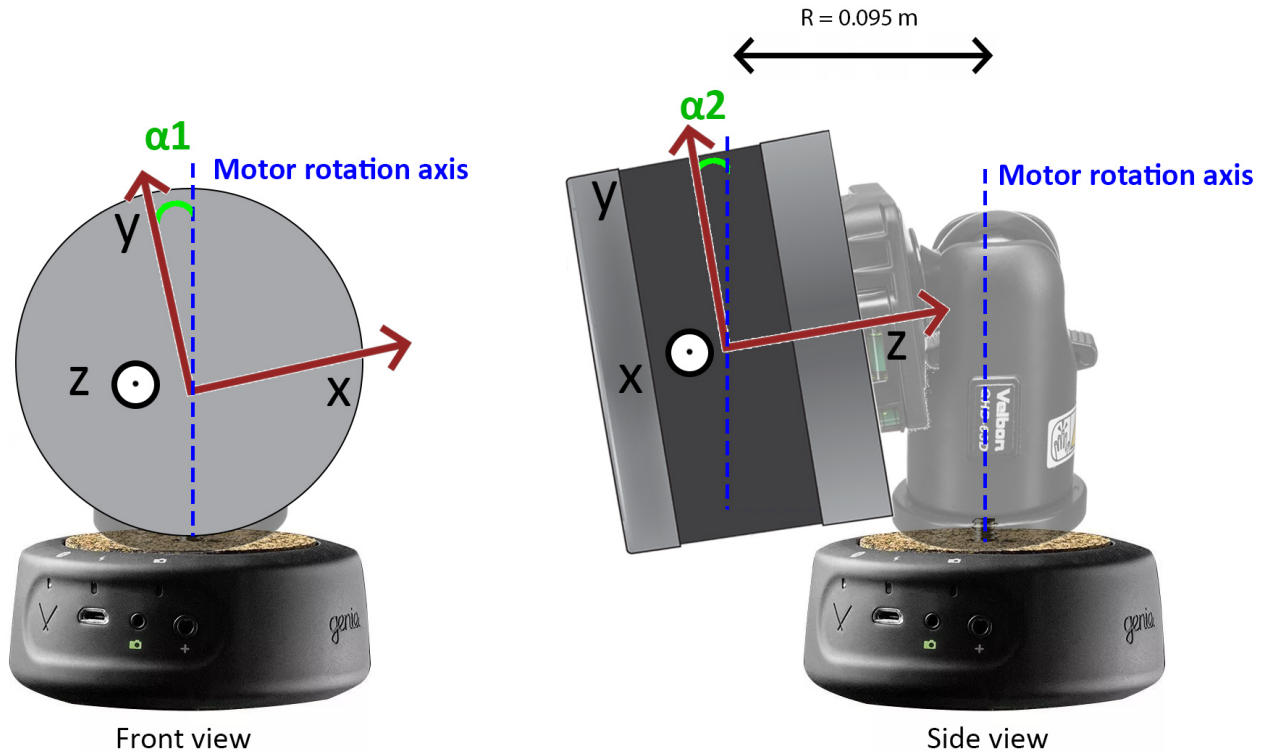
Figure 4. two possible angles between the system and the rotation axis

90   that the lidar is positioned on a ball head and a L-shaped liece, it is shifted from the rotation axis. This distance was manually measured as 0.095 m, and for each frame a translation on the z axis was applied. The affine transformation is a matrix presented as follows:

$$T_2 = \begin{bmatrix} 1 & 0 & 0 & 0 \\ 0 & 1 & 0 & 0 \\ 0 & 0 & 1 & 0 \\ 0 & 0 & 0.095 & 1 \end{bmatrix}$$

Another important consideration is that during the alignment of the frames, we have supposed that the Cartesian's coordinate system is the same as that of the motor. In fact, those two systems are different because the material is assembled by hand, which implies inaccuracies. Figure 4 shows the two possible angles α_1 and α_2 between the system and the rotation axis. The manual adjustment of those two systems involves an offset that highly influence the point cloud geometry if uncorrected. As these offsets cannot be measured manually, an automatic calibration is performed in post-treatment.

To find α_1 and α_2, the Nelder-Mead optimization algorithm is used, which is based on minimizing a continuous function using a simplex of dimensions equivalent to the number of parameters (Lagarias et al., 1998). At each iteration, a point located near the initial simplex is generated involving a new sample if a minimum is found, until convergence.

The resolution of the densified scan is not regular. Indeed the point cloud resolution is very high near the lidar scanner and decreases away from the sensor. Because the algorithms for measuring the distance between two sets of point clouds require a lot of computer resources and must be repeated at each iteration of the Nelder-Mead optimization, the scans are downsampled to an uniform resolution. In addition, the optimization is carried out only for points within the distance range in the best accuracy range of 3 to 7 metres (Glennie et al., 2016).

The optimization seeks to obtain the α_1 and α_2 angles that minimize two functions:

1. During the rotation of the motor, the entire scene is recreated for each of the 16 scan lines. These identical images are then put back together to form a dense point cloud. The overlap of the images is influenced by changing the angle α_1 . Thus, the function to be minimized corresponds to the average distance between all images produced by the scan lines 1 to 16.

2. The second function determines the angle α_2, based on the observation that both sets of symmetrical point clouds produced during the rotation must be exactly superposed. The variation of the angle α_2 creates a doming effect that tends to increase the average distance between both point clouds (figure 5). α_2 is determined by minimizing this distance.

3.3 Effect of the calibration and performance of the system

Visually, a wrong calibration of α_1 results in blur around the scanned image. A wrong calibration of the α_2 angle results in a doming effect that increases away from the center. To illustrate this, several scans were carried in a building of the University of Lausanne. A corridor of dimension 23 by 1.5 meters was scanned and a plan was fitted on the floor surface which is known to be horizontal. This plan is based on a distance interval to the lidar equivalent to the best accuracy range, i.e. between 3 and 7 meters depending on the lidar performance tests (Glennie et al., 2016). This avoids the influence of points too close or too far away, which can distort the theoretical equation of the plan. In addition, the points selected for fitting the plan come from an adequate sub-sampling of the initial scan in order to standardize the density of points over the distance interval. Then, the distance of all points to this theoretical plan are evaluated, which gives us an indication of the distribution of errors. Evaluation of the error as a function of the scanning distance was also measured.

Finally, a reproducibility test was performed for different motor speeds. The same scene was scanned several times to estimate the average distance between the point clouds. For that the Cloud to cloud Distance Tool with default parameters was performed in CloudCompare.

Geoscientific
Instrumentation
Methods and
Data Systems
Discussions

Open Access

EGU

3.4 Testing the system in different environments

The system has been tested in various environments. For all scans performed, the Syrp Genie Mini has been configured to rotate
360 degrees in 6 minutes. These parameters allowed the acquisition of high points resolution to maximize the information
collected while maintaining a reasonable scan time. With this setting, about 10 millions points per scan are collected. The
first tests were carried out in a building of the University of Lausanne is characterized by vast surfaces and volumes. Then,
the system was then used in a confined environment with no available GNSS signal: the Baulmes mines, a limestone mine
disaffected at the end of the Second World War.

In these environments, several scans were assembled using the iterative closest point (ICP) alignment algorithm (Besl, P. J.,
McKay in 1992). This is the most popular method alignment approach for point clouds, which searches for nearest neighbors
to minimize the distance between two point clouds. Thus, several scans from different points of view are assembled into a
single point cloud without the use of GNSS.

3.5 Comparison with a high-cost system

The TLS was compared with an acquisition made with the ZEB-REVO from Geoslam. This system falls into the high-cost
category and can record 40,000 points per second and aligns them using a SLAM algorithm with an accuracy of 15 mm
according to manufacturers. This device has the advantage of not depending on a GPS connection for alignment, but is limited
by its range of only 30 meters. Thus, two scans representing the same scene were performed indoors with both systems. The
two scans were then registred in CloudCompare using the ICP algorithm (with default parameters). Then, the Cloudcompare
"Cloud to cloud distance" tool (with default parameters) was applied to measure the distance between the two point clouds.

4 Results

All point clouds are visualized in the CloudCompare software. An EDL (Eye Dome lighting) shading filter allowing the creation
of real-time shading has been applied for better visualization (CloudCompare, 2019).

4.1 Effects of calibration

Figure 5 shows the the quality of a scan that was carried out indoors in a work area of the University of Lausanne.

Figure 5a shows the scene after the alignment of the different frames produced by the VLP-16 during the scan. A kind of
blur caused by the splitting of the scene is observed. No processing has yet been done, so the parameters α_1 and α_2 are set to
0.

Figure 5b shows the scene after applying the calibration parameters defined using automatic calibration; however, a slight
blur is still present, which is caused by the overlapping of points from both halves of the lidar scan that are not perfectly
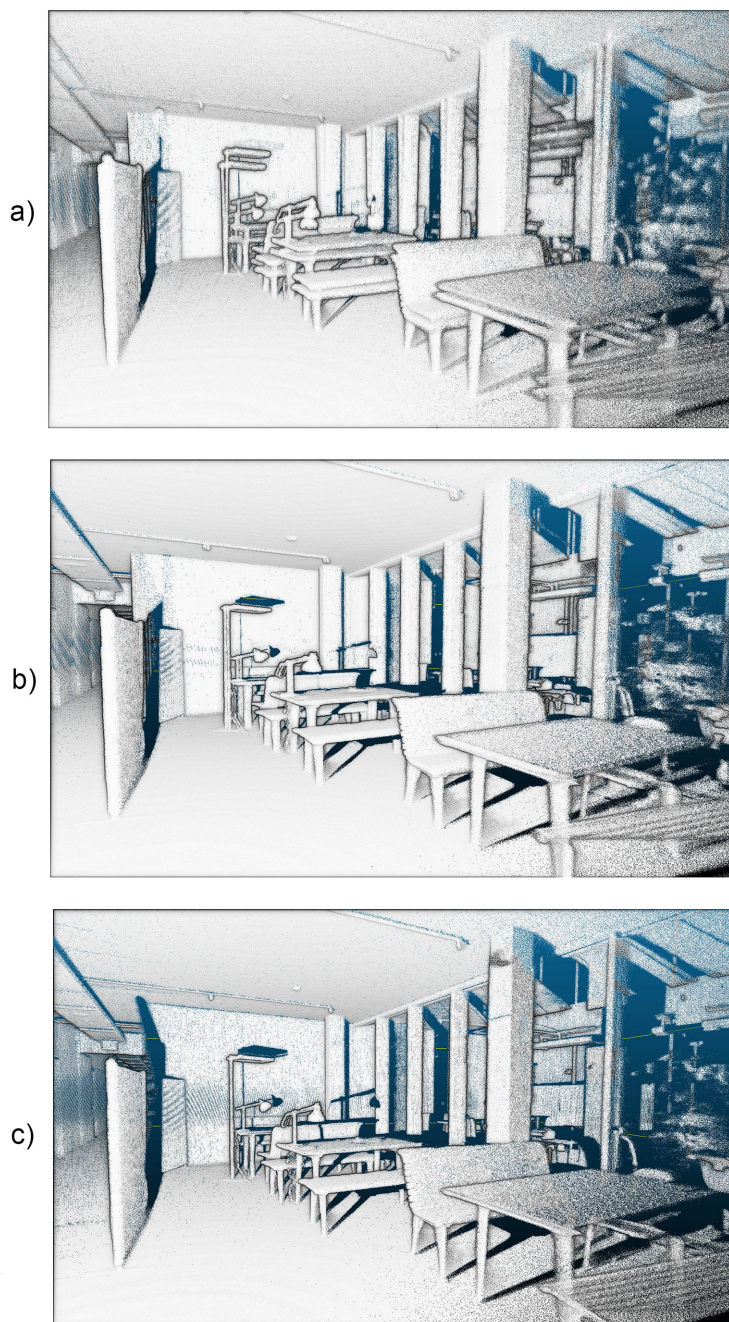aligned.

Geoscientific
Instrumentation
Methods and
Data Systems
Discussions

Open Access

EGU

Figure 5. Visualization of the calibration effects: (a) Scan without calibration, (b) Scan after calibration of α_1 and α_2, (c) Scan after post-treatment

Geoscientific
Instrumentation
Methods and
Data Systems
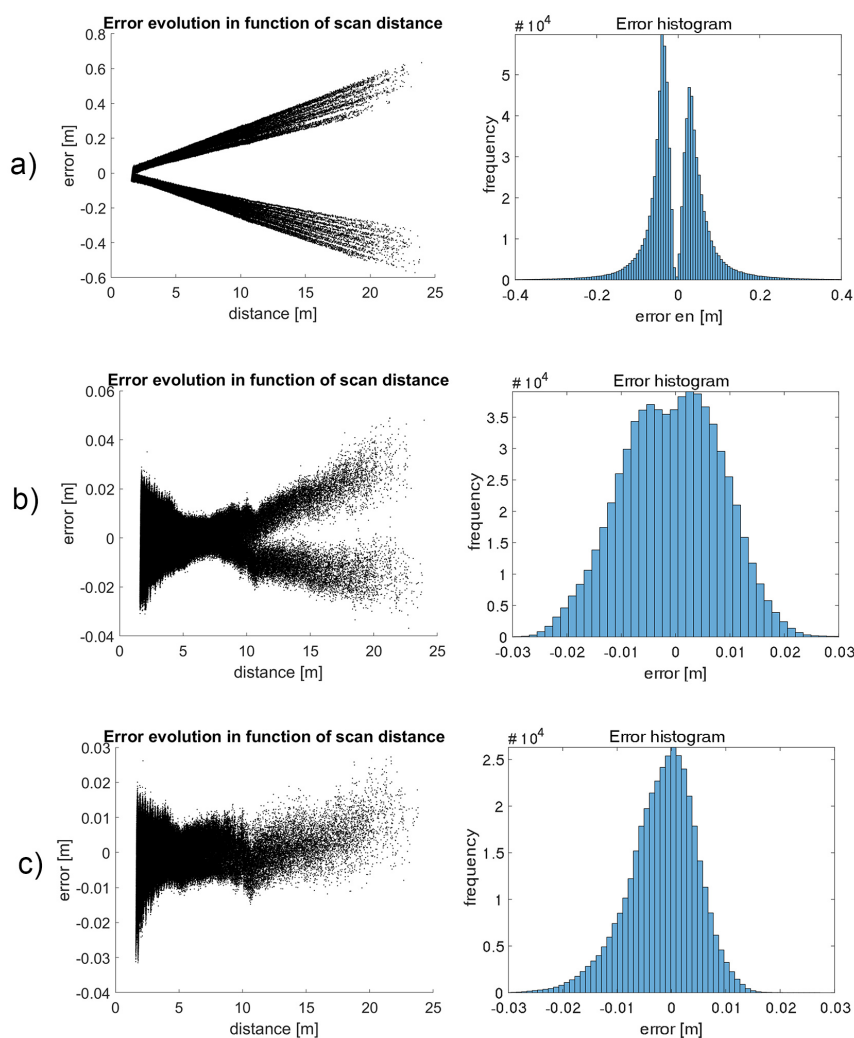Discussions
Open Access

Figure 6. Effects of calibration in relation to a theoretical plan : (a) Error estimation before calibration, (b) Error estimation after calibration, (c) Error estimation after post-treatment

Figure 5c shows the scene where only the scanned points corresponding to the positives coordinates on the x-axis are displayed (i.e., 50% of the data are discarded). In addition, a sub-sampling at 0.005m is applying and a noise filtering is performed.

160 Figure 6 shows the error corresponding to the distance of the points from the theoretical plane and the error histogram for the three calibration steps respectively.

Geoscientific
Instrumentation
Methods and
Data Systems
Discussions

4.2 Densification quality

Figure 7a gives an overview of a scan performed indoors after calibration. A photograph of the scanned scene with the same viewing angle is shown in figure 7b

165   Figures 8a and 8b show two previews of scans performed at the Baulmes mines.

Figure 8c shows the result of the registration of 4 point clouds in the Baulmes mines. The points corresponding to each of the acquisitions are represented in a different color to highlight the registration. It should be noted that the clouds have not been cleaned to removed artifacts, so we can see that the sensor has scanned itself. The results are characterized by a spacing set at 0.005 meters and is visually realistic.

170   Table 3 shows the ability of the system to reproduce the same point cloud at four rotation speeds. For each speed, two scans were performed and the distance between them is evaluated. The average distance and standard deviation between all points are calculated.

Table 3. Reproducibility test for 4 scanning speed

Scan time	36s	1min	2min	6min
Mean distance [m]	0.0581	0.0167	0.0145	0.0108
Standard deviation [m]	0.169	0.0248	0.132	0.0343

To validate the registration, the calculation of the distances between the points coming from the assembly and those coming from GeoSLAM were done using CloudCompare with the option "Cloud to cloud distance". The average distance between

175   both point clouds and the standard deviations of these distances are shown in Table 4.

Table 4. Mean distance and Std. between the Geoslam and velodyne TLS

|	Average distance [m]	Std. [m]
Before cleaning	0.0616	0.1991
After cleaning	<0.02	—

The calibration parameters for the indoors scans is shown in table 5. Table 6 shows the calibration parameters for the scans made in the Baulmes Mines.

Table 5. Summary of calibration parameters

Indoor scan	Calibration α_1	Calibration α_2
Scan 1	1.057	0.079
Scan 2	-0.631	0.347
Scan 3	-0.351	0.296
Scan 4	-1.061	-1.087

a)
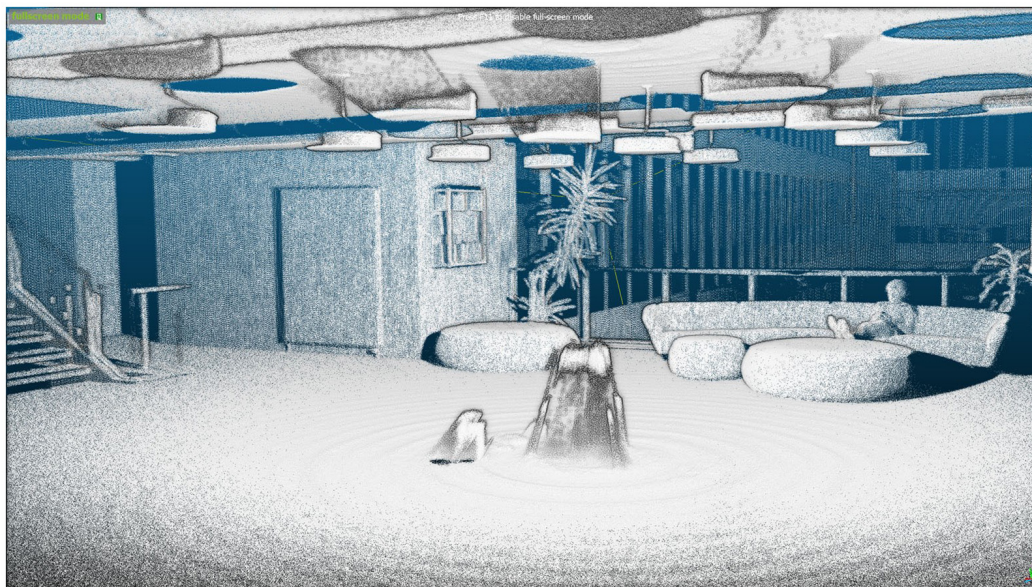
b)

Figure 7. Example of point cloud densification after calibration of the system : (a) Result of an indoor point cloud densification, (b) Picture of the scene
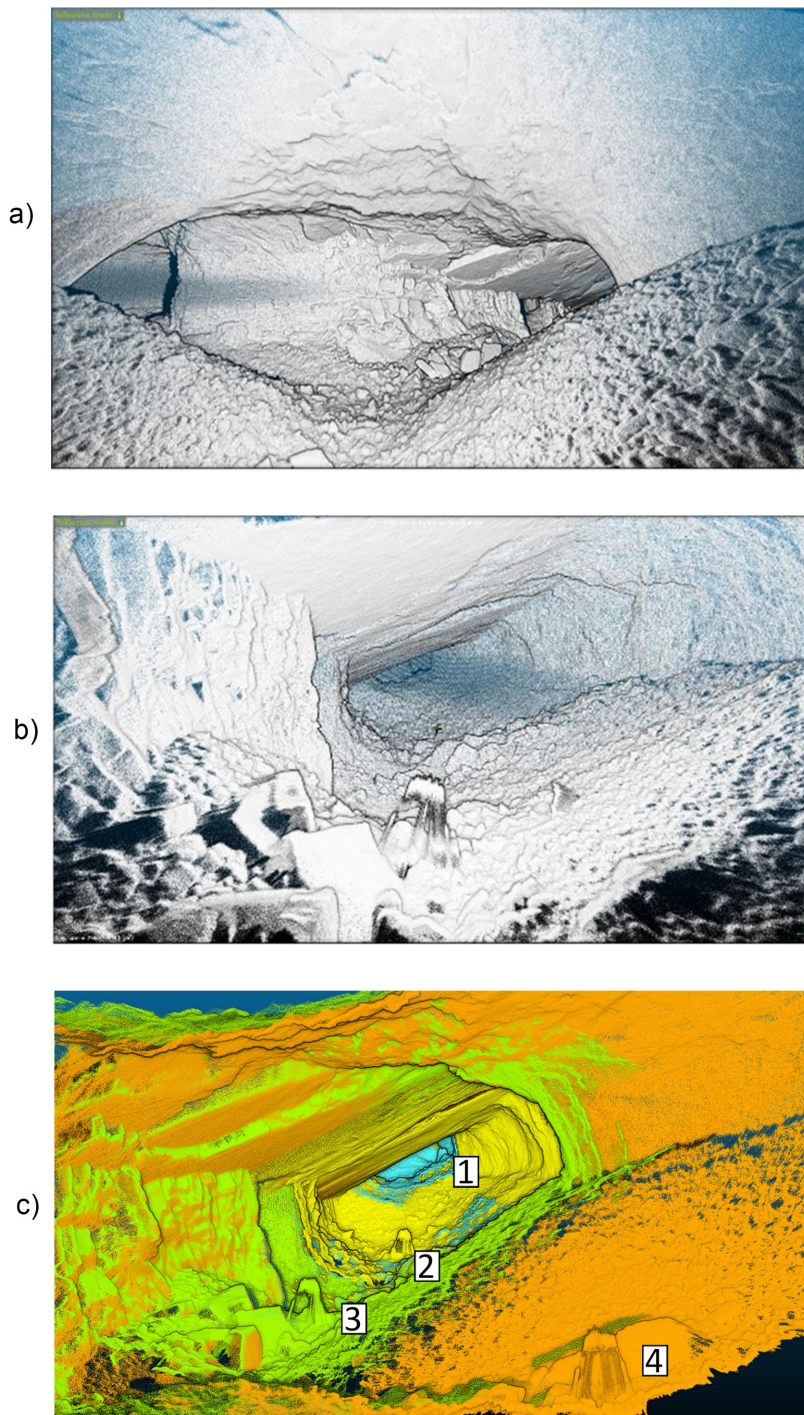
Geoscientific
Instrumentation
Methods and
Data Systems
Discussions

Open Access

Figure 8. Scanned scenes in Baulmes mines. The height of the gallery is about 3.5 m : (a) Mine example 1, (b) Mine example 2, (c) Point cloud registration in the mine

Geoscientific
Instrumentation
Methods and
Data Systems
Discussions

Table 6. Summary of calibration parameters

Mines scan	Calibration α_1	Calibration α_2
Scan 1	-0.734	0.001
Scan 2	-1.279	-0.191
Scan 3	-1.313	-0.307
Scan 4	-1.164	-0.307
Scan 5	-0.704	-0.280

A close range artifact has been observed after the reconstruction of the scenes. Figure 9 illustrates this artifact, which is characterized by wavelets near the system that fade away with distance.

5 Discussion

5.1 Data analysis before and after calibration

As shown in Figure 5, calibration is a fundamental step in producing accurate 3D modeling of an environment.

The use of the two symmetrical datasets produced during an acquisition using the VLP-16 is a key element in the optimization of the system. However, as shown in Figure 5b, it is difficult to determine the calibration parameter accurately because it implies a slight deformation in the reconstruction of the point cloud. For this reason, we decided to keep only half of the points (Figure 5c) in order to obtain a sharper representation of the scene. This choice will be justified after the analysis of the following results.

The error depends on the distance to the lidar. Before calibration, the distance to the theoretical plane varies from about $\pm$ 4 cm for the closest points to the lidar to 59 cm for a scan distance of 23 m (figure 6a). After calibration of parameters α_1 and α_2, the entire point cloud approaches the theoretical surface, as shown in Figures 6b. However the evolution of the error as a function of distance is still not constant, being about $\pm$ 2.5 cm for the points closest to the lidar, dropping to about $\pm$ 1 cm at a distance of 7.5 m, and eventually reaching $\pm$ 4 cm for a scan distance of 23 m. The minimum error is logically in the point range where the theoretical plan is situated. The bimodal error histogram shown in fibure 6b and (centred at $\pm$ 0.5 cm) shows that the superposition between the two halves of the scan is still not entirely accurate despite the calibration performed.

The evolution of the error as a function of the scanning distance when keeping only the half of the scan (figure 6c) shows an accuracy range of $\pm$ 2.5 cm, which remains within the accuracy range proposed by Velodyne.

5.2 Performance and stability of the TLS

According to the manufacturer's website, the VLP-16 Puck allows data acquisition at a distance of 100 m for an accuracy of $\pm$ 3 cm, under optimal acquisition conditions. Various stability tests have been carried out in metrology laboratory, which indicate an accuracy of $\pm$ 2 cm for an acquisition distance of 5 meters to a white and flat target (Glennie, et al., 2016). The

Geoscientific
Instrumentation
Methods and
Data Systems
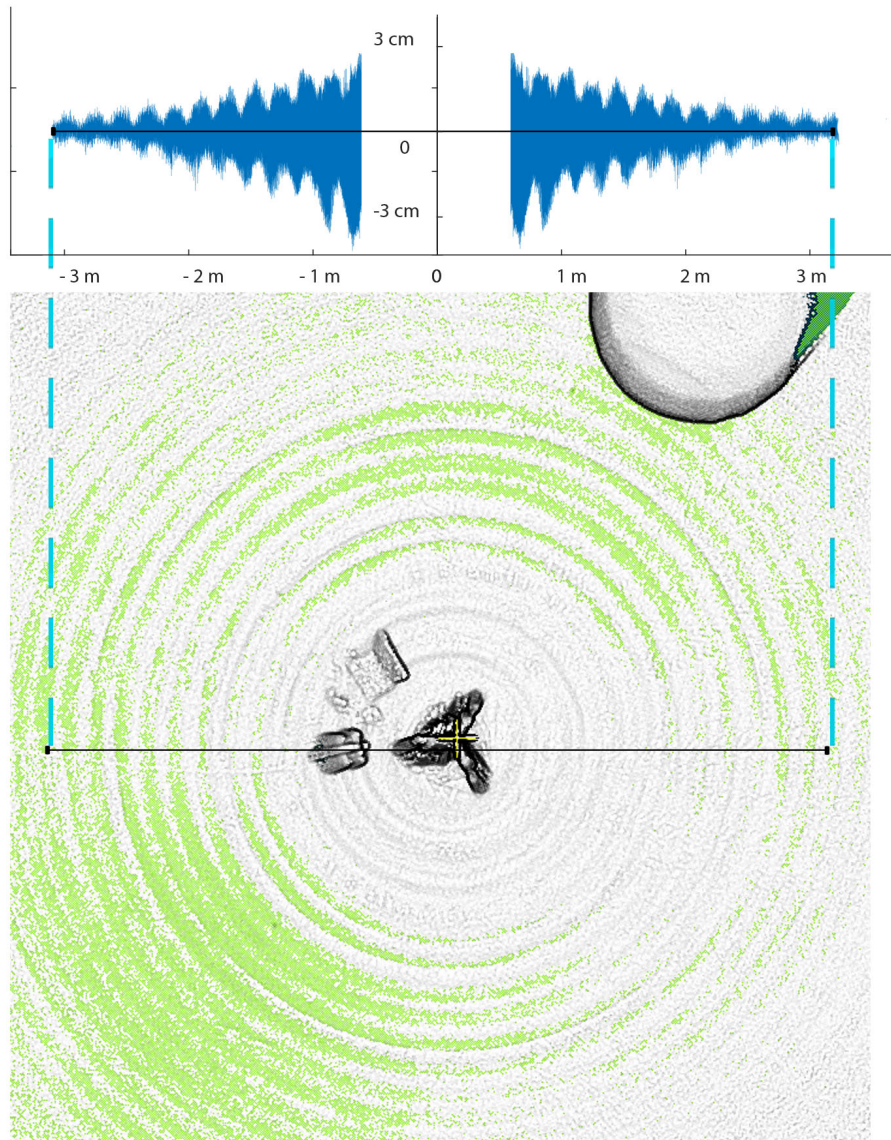
Discussions

Open Access

Figure 9. Artifact present near the TLS and its corresponding amplitude

tests carried out during this study made it possible to evaluate the performance of the lidar against a theoretical plan produced using a scanned flat surface (the central corridor of a building).

Reproducibility tests of the measurements made for scan speeds ranging from 36 seconds to 6 minutes show us that the motor speed must be as low as possible to increase the quality of the measurements.

205 The post-processing steps and the calibration of mounting angles has allowed to drastically reduce errors; however, the calibration parameters vary greatly between scans, as shown in table 5 and table 6. This can be explained by the assembly of our lidar system being relatively unstable. The impact of the calibration, and particularly the need to repeat the calibration for each scan, could be alleviated by welding together the different components of the system.

5.3 Comparison with more expensive hardware

210 The generation of dense and accurate scans allowed the use of an ICP algorithm for point clouds registration. After comparing the scans performed with the Geoslam, superposition of ± 2 cm is present, which shows that the two scans overlap well. Some areas where the distance between the two scans is more than 10 cm correspond to the presence of people during the acquisition with GeoSLAM (table 6).

5.4 Origin of the short-range artifacts

215 Visually, this artifact is easily observed in the results of scans near the tripod,when data acquired on a flat surface. Figure 9 shows the influence of this artifact on the scan. We notice that the error spreads in the form of regular waves and fades away as it moves away from the lidar. It has a magnitude of 3 cm at the closest to the lidar and drops below 1.5 cm at a distance of 3m. The wave frequency is about 20cm. A hypothesis on the origin of this artifact would be related to the length of the arm which was measured manually. After various tests, it turns out that errors in the length of the arm has no influence on the
220 occurrence of these artifacts, but instead creates horizontal deformations. Another hypothesis is that the artifacts are related to the scanning speed of the lidar system. However, the artifacts remain constant (same distance and amplitude between waves) despite changes in engine rotation speeds. This tells us that the artifacts seem to be related to the lidar itself. Since the error appears to be regular, it would be conceivable to correct outliers by modifying each point according to the distance to the lidar.

6 Conclusion

225 As shown in the results, our system requires calibration for each scan performed. Optimization of the equipment, such as the use of a more accurate engine, is possible for such a project and could improve the quality of the measurements while maintaining a low-cost aspect. The results obtained with this system are satisfactory. The use of the lidar system in a mine has proven its ability to be independent of a GPS referencing system. Comparison with a high-cost system using a SLAM alignment algorithm verified the quality of registration. A follow-up to this study could be the validation of the performance
230 of this system using a total station survey. The use of this lidar system on mobile supports is possible with the addition of an inertial station. This study has shown that TLS allows high and accurate data production can be used at a lower cost.

Geoscientific
Instrumentation
Methods and
Data Systems
Discussions

Open Access

EGU

Code availability. Velodyne TLS

GitHUB repository

Data availability.

235 *Code and data availability.*

Sample availability.

Video supplement.

Baulmes

Reclere

240 Milandre

Rolex Learning Center

Appendix A

A1

Author contributions. JB developed the methodology, carried out the field experiments and wrote the manuscript, MHD provided advice and
245 methodological guidance and contributed to the manuscript, GM proposed the initial framework, provided supervision and contributed to the
manuscript

Competing interests.

Disclaimer.

References

Ackermann, F.: Airborne laser scanning—present status and future expectations, ISPRS Journal of Photogrammetry and Remote Sensing, 54(2–3), 64–67, doi:10.1016/S0924-2716(99)00009-X, 1999.

Barnea, S. and Filin, S.: Keypoint based autonomous registration of terrestrial laser point-clouds, ISPRS Journal of Photogrammetry and Remote Sensing, 63(1), 19–35, doi:10.1016/j.isprsjprs.2007.05.005, 2008.

Davis, P. A.: The Analysis of Lidar Signatures of Cirrus Clouds, Appl. Opt., 8(10), 2099, doi:10.1364/AO.8.002099, 1969.

Geiger, A., Lenz, P. and Urtasun, R.: Are we ready for autonomous driving? The KITTI vision benchmark suite, in 2012 IEEE Conference on Computer Vision and Pattern Recognition, pp. 3354–3361., 2012.

Glennie, C. L., Kusari, A. and Facchin, A.: Calibration and stability analysis of the VLP-16 laser scanner, Int. Arch. Photogramm. Remote Sens. Spatial Inf. Sci., XL-3/W4, 55–60, doi:10.5194/isprs-archives-XL-3-W4-55-2016, 2016.

Jaboyedoff, M., Oppikofer, T., Abellán, A., Derron, M.-H., Loye, A., Metzger, R. and Pedrazzini, A.: Use of LIDAR in landslide investigations: a review, Nat Hazards, 61(1), 5–28, doi:10.1007/s11069-010-9634-2, 2012.

Lagarias, J. C., Reeds, J. A., Wright, M. H. and Wright, P. E.: Convergence Properties of the Nelder–Mead Simplex Method in Low Dimensions, SIAM J. Optim., 9(1), 112–147, doi:10.1137/S1052623496303470, 1998.

Laurent, A., Moret, P., Fabre, J. M., Calastrenc, C., Poirier, N.: La cartographie multi-scalaire d'un habitat sur un site accidenté: la Silla del Papa (Espagne), 2019.

Mada, S. K., Smith, M. L., Smith, L. N. and Midha, P. S.: Overview of passive and active vision techniques for hand-held 3D data acquistion, edited by A. Shearer, F. D. Murtagh, J. Mahon, and P. F. Whelan, pp. 16–27, Galway, Ireland., 2003.

Northend, C. A., Honey, R. C. and Evans, W. E.: Laser Radar (Lidar) for Meteorological Observations, Review of Scientific Instruments, 37(4), 393–400, doi:10.1063/1.1720199, 1966.

Pouliot, J.: GMT-7006: Modelisation et Geovisualisation 3D. Universite Laval, departement des sciences geomatiques, 2018.

Royán, M. J., Abellán, A., Jaboyedoff, M., Vilaplana, J. M. and Calvet, J.: Spatio-temporal analysis of rockfall pre-failure deformation using Terrestrial LiDAR, Landslides, 11(4), 697–709, doi:10.1007/s10346-013-0442-0, 2014.

Schuster, B. G.: Detection of tropospheric and stratospheric aerosol layers by optical radar (Lidar), Journal of Geophysical Research (1896-1977), 75(15), 3123–3132, doi:10.1029/JC075i015p03123, 1970.

Shackleton, J., VanVoorst, B. and Hesch, J.: Tracking People with a 360-Degree Lidar, in 2010 7th IEEE International Conference on Advanced Video and Signal Based Surveillance, pp. 420–426., 2010.

Shan, J. and Toth, C. K.: Topographic laser ranging and scanning: principles and processing, Second edition., Taylor Francis, CRC Press, Boca Raton., 2018.

Stöcker, C., Nex, F., Koeva, M. and Gerke, M.: Quality assessment of combined IMU/GNSS data for direct georeferencing in the context of UAV-based mapping, Int. Arch. Photogramm. Remote Sens. Spatial Inf. Sci., XLII-2/W6, 355–361, doi:10.5194/isprs-archives-XLII-2-W6-355-2017, 2017.

Teza, G., Galgaro, A., Zaltron, N. and Genevois, R.: Terrestrial laser scanner to detect landslide displacement fields: a new approach, International Journal of Remote Sensing, 28(16), 3425–3446, doi:10.1080/01431160601024234, 2007.

Wang, Z., Liu, Y., Liao, Q., Ye, H., Liu, M. and Wang, L.: Characterization of a RS-LiDAR for 3D Perception, in 2018 IEEE 8th Annual International Conference on CYBER Technology in Automation, Control, and Intelligent Systems (CYBER), pp. 564–569, IEEE, Tianjin, China., 2018.